ORNL/CON–407

ornl

OAK RIDGE NATIONAL LABORATORY

LOCKHEED MARTIN

Performance of Powder-Filled Evacuated Panel Insulation in a Manufactured Home Roof Cavity: Tests in the Large Scale Climate Simulator

T. W. Petrie
J. Kośny
P. W. Childs

MANAGED AND OPERATED BY
LOCKHEED MARTIN ENERGY RESEARCH CORPORATION
FOR THE UNITED STATES
DEPARTMENT OF ENERGY

TABLE OF CONTENTS

LIST OF FIGURES

TABLES

ACKNOWLEDGMENTS

The authors are grateful for many fruitful technical discussions with our colleagues J. E. Christian and A. O. Desjarlais during the course of the tests and preparation of this report. Also acknowledged is the help provided by R. S. Graves and F. J. Weaver of the ORNL Metals & Ceramics Division in doing careful calibrations of the heat-flux transducers and additional tests for the effect of compression on the thermal conductivity of the fiberglass batts used in the tests. D. W. Yarbrough of the Metals & Ceramics Division and Tennessee Technological University provided a thorough review of the report and helpful suggestions from the perspective of the outdoor tests of whole manufactured homes that are being conducted at TTU as part of the CRADA that supported this work. G. J. Andrews, a graduate student at Tennessee Technological University, assisted with conducting and analyzing the tests with blown-in rock wool insulation.

ABSTRACT

A full-scale section of half the top of a single-wide manufactured home has been studied in the Large Scale Climate Simulator (LSCS) at the Oak Ridge National Laboratory. A small roof cavity with little room for insulation at the eaves is often the case with single-wide units and limits practical ways to improve thermal performance. The purpose of the current tests was to obtain steady-state performance data for the roof cavity of the manufactured home test section when the roof cavity was insulated with fiberglass batts, blown-in rock wool insulation or combinations of these insulations and powder-filled evacuated panel (PEP) insulation. Four insulation configurations were tested: A, a configuration with two layers of nominal R_{US}-7 h·ft²·°F/BTU (R_{SI}-1.2 m²·K/W) fiberglass batts; B, a layer of PEPs and one layer of the fiberglass batts; C, four layers of the fiberglass batts; and, D, an average 4.1 in. (10.4 cm) thick layer of blown-in rock wool at an average density of 2.4 lb/ft³ (38 kg/m³). Effects of additional sheathing were determined for Configurations B and C. With Configuration D over the ceiling, two layers of expanded polystyrene (EPS) boards, each about the same thickness as the PEPs, were installed over the trusses instead of the roof. Aluminum foils facing the attic and over the top layer of EPS were added. The top layer of EPS was then replaced by PEPs.

The high R-value PEPs fit easily between the trusses. When placed on a layer of fiberglass batts, they did not cover the ceiling joists. Moreover, the length of the PEPs caused joint effects; it took three panels between each pair of joists to span the distance from eave to ridge. Unlike the configurations with only fiberglass batts, PEPs caused no significant compression of insulation at the eave edge of the test section. The rock wool was not compressed at the eave edge and covered the joists well, but was not as thick near the eave or ridge edges as in the middle of the test section. System R-values measured for the whole test section showed the effects of these features. The system R-values were significantly less than the center-of-cavity R-values. Ratios of system to center-of-cavity R-values varied from under 50% with the PEPs, because of eave edge, joist and joint effects, to over 90% for two layers of fiberglass batts at summer conditions, where the metal roof had a radiant barrier effect.

We tried to improve the system R-values. With Configuration B, the system R-value was 23% better with sheathing over the eave edge and over most of the underprotected joists and joints than without it. Vertical sheathing at the eave edge improved the system R-value for Configuration C by 9%. Placing the layers of EPS over the entire roof area did not yield a commensurate increase in system performance with Configuration D because the eave edge was left thermally underprotected. The foil facing the attic space helped, especially at summer conditions. PEPs instead of one layer of the EPS were not successful either in significantly improving system R-value because of effects at the eave edge. Only when the entire eave edge was protected by wide EPS boards did a 51% improvement at the mid-winter condition and a 95% improvement at the summer condition occur in system R-value relative to the system R-value for the base-case tests with Configuration D.

Modeling of the base-case fiberglass batt and rock wool configurations and the PEPs on top of fiberglass batts with a three-dimensional conduction program predicted that 13 to 16% of the total heat

flow through the system area was across the thermally underprotected eave. The eave area for the model was 8.4% of the total system area, comprising 3.2% from the stub wall area and 5.2% from ceiling area to include the region where the two layers of fiberglass batts were compressed between the roof and ceiling. For the PEPs over fiberglass batts, further modeling showed that about half the decrease in R-value for the ceiling away from the eave edge relative to the center-of-cavity R-value was due to poor coverage of the joists. Modeling was also used to explore the benefits of improved thermal protection for the edge made possible by different construction techniques. A whole house model put the results for the roof cavity into the perspective of the annual heating and cooling energy needs of a whole single-wide unit.

The PEPs available for the tests achieved R_{US}-16 $h \cdot ft^2 \cdot °F/BTU$ (R_{SI}-2.8 $m^2 \cdot K/W$) in 0.79 in. (20 mm) thickness. This is very good center-of-cavity performance. The measurements of system R-value with PEPs between the trusses on top of a layer of fiberglass batts showed too many thermal shorts to take economic advantage of the high center-of-cavity R-value. The measurements of system R-value with insulation over the trusses showed potential for improving thermal performance of the roof cavity if the eave edge is improved simultaneously. PEPs could have application near the eave edge where space is very cramped if they can be installed without danger of damage to them. This danger is not easy to avert because there are strict requirements for strapping the roof to the side walls. For the near term, conventional sheathing, as much as can be tolerated, is recommended over the walls and the eave edge of the trusses.

EXECUTIVE SUMMARY

During the initial phase of work under CRADA ORNL 93-0191, a test section was designed that models 12 ft (3.7 m) of half the roof of a single-wide manufactured home with a pitched metal roof. The test section was built, instrumented and used in the Large Scale Climate Simulator (LSCS) in the Buildings Technology Center (BTC) at the Oak Ridge National Laboratory (ORNL). The LSCS allows conditions of temperature and humidity to be imposed above horizontal test sections to simulate outdoor conditions ranging from extreme winter to extreme summer conditions. Corresponding indoor conditions below the test sections can be set. The outdoor conditions can be varied to simulate diurnal variations. For this work, constant temperatures were imposed for sufficient times to achieve steady-state. Figure 1ES shows schematically the manufactured home test section in place in the LSCS.

The purpose of the tests was to obtain steady-state performance data for the roof cavity of this single-wide manufactured home. Our industrial partner in this CRADA built the test section with materials and tools used in their regular production of manufactured homes. We installed guard insulation around the perimeter of the test section (shown as cross-hatched area in Fig. 1ES) to minimize flanking losses. The roof cavity was insulated with conventional insulation and with powder-filled evacuated panel (PEP) superinsulation. Four insulation configurations were tested: A, a configuration consisting of two layers of nominal R_{US}-7 h·ft²·°F/BTU (R_{SI}-1.2 m²·K/W) fiberglass batts; B, a configuration in which a layer of PEPs replaced one layer of the fiberglass batts; C, a configuration that used four layers of nominal R_{US}-7 fiberglass batts; and, D, blown-in rock wool insulation. Effects of additional sheathing at the eave edge and over joists and joints were determined for Configuration B and at the eave edge only for Configuration C. For Configuration D, two layers of expanded polystyrene (EPS) insulation, foils facing the attic space and over the top layer of EPS and then PEPs instead of the top EPS layer were installed over the trusses instead of the metal roof.

The test section was built to allow calorimetric determination of the total heat loss or heat gain through the assembly into the nominal 8 × 8 ft (2.4 m × 2.4 m) opening of the metering chamber of the LSCS. To ensure that the full effect of the underprotected eave edge was measured calorimetrically and to allow testing of modifications to it, the test section was built on stub walls like the actual side walls of the unit whose features were incorporated in the design of the test section. Only the heat flowrates through the ceiling and area of unguarded stub wall on the eave edge were desired from the metering chamber energy balance. The balance was corrected for flanking losses around the perimeter. For flanking losses through large, independently measured thermal resistances, temperature differences were measured and used with the thermal resistances to estimate the heat flow. The flanking losses through unknown thermal resistances were estimated from the response of calibrated heat-flux transducers in place around the perimeter.

Checks of the accuracy of the metering chamber energy balance were done as part of the tests. A calibration panel, comprising a 4 in. (10.2 cm) thick layer of EPS with known R-value, was inserted into

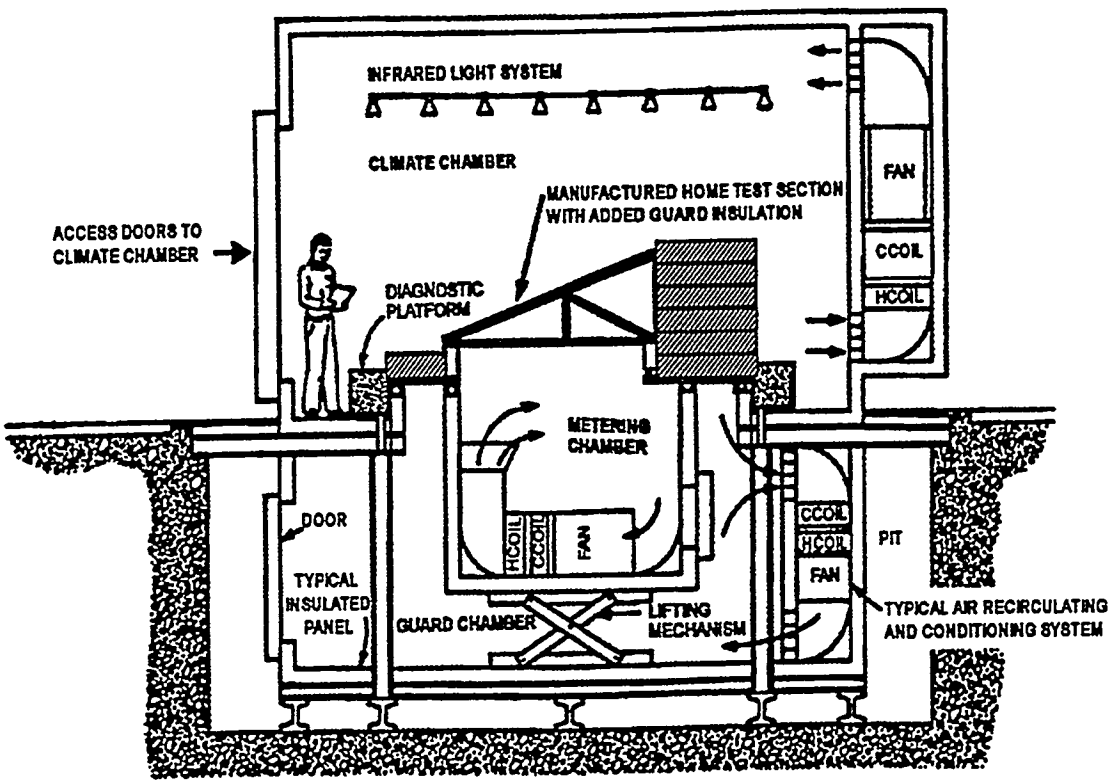

Fig. 1. (Executive Summary). Schematic of the manufactured home test section inside the Large Scale Climate Simulator.

the LSCS. The metering chamber balance reproduced the panel's known R-value of about 16 h·ft²·°F/BTU (2.8 m²·K/W) within ±0.1 h·ft²·°F/BTU (±0.02 m²·K/W) at mean insulation temperatures from 25 to 50°F (-4 to 10°C). At summer conditions cooling is required in the metering chamber. Overcooling allowed temperature to be controlled with the same heaters as used for winter conditions. With optimum cooling, R-values for the calibration panel were within ±0.3 h·ft²·°F/BTU (±0.05 m²·K/W) of known values at mean insulation temperatures from 85 to 100°F (29 to 38°C).

Three HFTs were especially calibrated for use inside the attic space of the manufactured home test section. Thermocouples were located beside each HFT and directly above them. This placement of HFTs and thermocouples gave data to measure the center-of-cavity R-value of the insulations and an apparent insulation R-value near the eave edge of the test section. The energy balance on the metering chamber is used to calculate an R-value for the system. For these tests, it is defined as

$$R_{system} = \Delta T \cdot A/Q \qquad \text{(1ES)}$$

where ΔT is the difference between the average air temperatures above and below the test section,
A is the inside surface area of the test section exposed to the metering chamber, and
Q is the net heat flow through this area, from the corrected metering chamber energy balance.

Because a correction is made for flanking losses around the perimeter of the test section, the area is taken as the sum of the ceiling area and the area of the stub wall above the guard insulation on the eave side. The ceiling area is 96 in. × 76.25 in. (2.44 m × 1.94 m) and the exposed stub wall area is 96 in. × 2.5 in. (2.44 m × 0.064 m), totaling 52.5 ft^2 (4.89 m^2). The stub wall contributes only 3.2% to the total area.

The insulation configurations with fiberglass batts or blown-in rock wool insulation in the roof cavity showed strong responses to the construction features of the test section, especially those at the eave edge of the roof. The systems consisting of a layer of fiberglass batts and PEPs on the ceiling or using blown-in rock wool were not affected by vertical compression of insulation at the eave. Insulation coverage was poor over the joists with PEPs on top of fiberglass batts because the panels had to fit between the vertical and slanted truss members. There were also joints between the three panels used from eave to ridge in each space between joists. The configurations comprising two and four layers of fiberglass batts had compressed insulation at the eave but insulation was continuous from eave to ridge. Joist coverage was not perfect because the semi-rigid batts could not conform only to where the vertical and slanted truss members joined the joists. The blown-in insulation was not compressed at the edge but its thickness there was not as great as in the middle of the test section because of the short heel at the eave edge. Thickness near the ridge edge was also less than in the middle because of the blowing technique that was used.

Thermal performance of the Configurations A, B, C and D is shown in the table. The ratios of the system to center-of-cavity insulation R-values show how much the system R-values are affected by insulation compression or reduced insulation at the eave edge, thermal bridges and effects through joists and joints.

Configuration	Condition	Center-of-Cavity R_{US} (R_{SI})	System R_{US} (R_{SI})	System/Center (%)
A. Two FG Batts	Winter	15.6-17.2 (2.7-3.0)	12.0-12.4 (2.1-2.2)	72-77
	Summer	13.2 (2.3)	12.1 (2.1)	92
B. PEPs on FG	Winter	24.1-25.8 (4.2-4.5)	12.4-12.7 (about 2.2)	49-53
	Summer	---	---	---
C. Four FG Batts	Winter	30.4-31.7 (5.4-5.6)	16.8-18.6 (3.0-3.3)	55-59
	Summer	27.6 (4.9)	15.8 (2.8)	57
D. Rock Wool	Winter	13.0-14.0 (2.3-2.5)	9.1-10.1 (1.6-1.8)	65-74
	Summer	12.4 (2.2)	9.9 (1.8)	80

Improvements in system R-values were sought by improvements in Configurations B, C and D. After the initial tests with Configuration B, 0.75 in. (1.9 cm) thick extruded polystyrene (XPS) sheathing was installed over the eave edge and 4 in. (10.2 cm) thick EPS was installed over most of the underprotected joists and over the joints between the PEPs. The XPS and EPS sheathing improved the system R-value by 23% compared to the initial results with Configuration B. Vertical XPS sheathing at the eave edge improved the system R-value for Configuration C by 9%. Placing two EPS layers, each 0.625 in (1.6 cm) thick, over the trusses instead of the metal roof showed a 7 to 9% increase over the initial

system R-value with Configuration D. Adding an aluminum foil facing the attic space showed a 27% increase at winter conditions and a 29% increase at summer conditions relative to the initial results. Placing PEPs instead of one of the EPS layers over the trusses yielded 28% improvement over Configuration D at winter conditions and 51% at summer conditions. In all these cases, the eave edge was left thermally underprotected. The entire eave edge was then protected by wide EPS boards like the one shown in Fig. 1ES covering most of the stub wall. The combined effect of all improvements was a 51% higher system R-value at the mid-winter condition and a 95% higher one at the summer condition relative to the system R-values with the base-case Configuration D.

HUD manufactured housing construction and safety standards require compliance with an upper limit on the overall U value of the roof/ceiling, walls and floor. The limit varies with location, specified as one of four zones in the continental U.S. For the roof/ceiling, center-of-cavity insulation R-values and inside and outside film resistances, all at 75°F (24°C), are used with parallel path corrections for insulation compression and framing effects. The method is specified in a companion HUD manual. For this test section, including the stub wall on the eave edge, the system R-value for insulation Configuration A by this method is estimated to be R_{US}-14.8 (R_{SI}-2.6). This is 21% higher than the measured average of 12.2 for this system.

The eave edge, the space around a horizontal ceiling joist, and an entire 14 ft (4.3 m) wide × 52 ft (15.8 m) long manufactured home were modeled to provide insight to the measurements. For the two layer fiberglass batt insulation package and for the PEPs over fiberglass batts, the model of the eave edge showed that 16% of the total heat flow across the test section came across the eave edge. For the rock wool, the eave edge loss was 13% of its larger total. For the two-layer fiberglass batt and PEP configurations, the model of heat flow across a horizontal ceiling joist addressed only the joist effect in the ceiling R-values. The joist was away from the eave edge and free from connections to other truss members. Ceiling R-values were obtained from differences between measured total heat flows and predicted eave edge heat flows. For the PEPs, further modeling addressed the effects of sheathing over the joist. The blown-in rock wool was not modeled because it would not show a joist effect. The predictions yielded a joist effect of only 1% for the two layers of fiberglass batts but, since the PEPs did not cover the joists, about 18% and 23% for the PEPs on top of a layer of fiberglass batts with and without sheathing, respectively. The differences between the joist and total ceiling framing effects were about 20% for all of the insulation configurations meaning that the vertical and slanted truss members effectively reduced the system R-value by about 20% from the center-of-cavity insulation R-value. The blown-in rock wool showed a 21 to 32% framing effect for the ceiling, which is attributed to poorer coverage near the ridge edge and some effect of the vertical and slanted trusses.

The whole house computer simulation showed annual energy savings for proposed improvements in construction features of manufactured homes. Improving just the edge of the roof saved very little. But, if mechanical constraints would allow the extra width caused by 0.5 in. (13 mm) thick vertical XPS sheathing over all exterior walls and the eave edge, payback times for the sheathing were 2.5 to 4 years.

The PEPs available for the tests achieved R_{US}-16 h·ft^2·°F/BTU (R_{SI}-2.8 m^2·K/W) in 0.79 in. (20 mm) thickness. This is very good center-of-cavity performance. The measurements of system R-value with PEPs between the trusses on top of a layer of fiberglass batts showed too many thermal shorts to take economic advantage of the high center-of-cavity R-value. The measurements of system R-value with insulation over the trusses showed potential for improving thermal performance of the roof cavity if the eave edge is improved simultaneously. PEPs could have application near the eave edge where space is very cramped if they can be installed without danger of damage to them. This danger is not easy to avert because there are strict requirements for strapping the roof to the side walls. For the near term, conventional sheathing, as much as can be tolerated, is recommended over the walls and the eave edge of the trusses.

1. INTRODUCTION

During the initial phase of work under CRADA ORNL 93-0191, a test section was designed that duplicates 12 ft (3.7 m) of half the roof of a single-wide manufactured home with a pitched metal roof. The test section was built, instrumented and used in the Large Scale Climate Simulator (LSCS) in the Buildings Technology Center (BTC) at the Oak Ridge National Laboratory (ORNL). The LSCS allows conditions of temperature and humidity to be imposed above horizontal test sections to simulate outdoor conditions ranging from extreme winter to extreme summer conditions. Corresponding indoor conditions below the test section can be set. The outdoor conditions can be varied to simulate diurnal variations. For this work, constant temperatures were imposed for sufficient times to achieve steady-state.

The purpose of the tests was to obtain steady-state performance data for the half-roof assembly when the roof cavity was insulated with combinations of conventional insulation and powder-filled evacuated panel (PEP) superinsulation. Four insulation configurations were tested: A, a configuration consisting of two layers of nominal R_{US}-7 h·ft²·°F/BTU (R_{SI}-1.2 m²·K/W) fiberglass batts; B, a configuration in which a layer of PEPs replaced one layer of the fiberglass batts; C, a configuration that used four layers of nominal R_{US}-7 fiberglass batts; and, D, blown-in rock wool insulation. Effects of additional sheathing at the eave edge and over joists and joints were determined for Configuration B and effects of sheathing at the eave edge only for Configuration C. After base-case tests with Configuration D, two layers of expanded polystyrene (EPS) insulation were installed over the trusses instead of the metal roof. Then aluminum foils facing the attic cavity and over the top layer of EPS were added. Finally, PEPs replaced the top layer of the EPS. The performance of superinsulation compared to that of the base-case fiberglass batt and rock wool configurations in the relatively small LSCS test sections is of interest for two reasons. First, it foretells the energy conserving potential of manufactured homes built with superinsulated tops. Second, it guides the whole roof and whole house outdoor tests that make up the work planned for later phases of this CRADA by our university partner.

2. CONSTRUCTION FEATURES OF THE TEST SECTION

The test section for use in the LSCS is designated as the manufactured home test section. Figures 1 and 2 show, respectively, a photograph and a scale drawing of an end view and a side view. The overall dimensions of the test section are 12.5 ft long × 12.5 ft wide × 2.7 ft high (3.8 m × 3.8m × 0.83 m). The halves of the roof trusses are only 6.8 ft (2.1 m) wide, corresponding to the width of half the roof of a 14 ft (4.3 m) wide manufactured home. Oriented strand board (OSB) extensions allowed the test section to rest on 0.75 in. (1.9 cm) thick extruded polystyrene (XPS) foam insulation strips atop the 5 in. (13 cm) wide lower ledge of a Z-frame for the diagnostic platforms that fit into the LSCS. In Fig. 1, the papers in the foreground lie on the diagnostic platform and the upper ledge of the Z-frame. A single layer of fiberglass batt insulation is in place in this picture. One PEP is on top of the fiberglass in the foreground. Three more layers of the batts are shown in the background. The PEP and extra three layers of batts allow direct comparisons of the center-of-cavity thicknesses of the configurations using fiberglass batts that were installed later. When the roof was installed over the trusses, it compressed any insulation that extended above the trusses.

Our industrial partner in this CRADA built the test section to the specifications shown in Fig. 2 with materials and tools used in their regular production of manufactured homes. Trusses for one of their 14 ft (4.3 m) wide units with a pitched metal roof and flat ceiling were cut exactly in half. The only significant deviation from actual construction practice was to allow the sheet metal roof to be removable so that we could install thermocouples and heat-flux transducers and change insulation configurations. We also installed the guard insulation shown in Fig. 2 around the perimeter of the test section.

The test section was built to allow calorimetric determination of the total heat loss or gain through the assembly into the nominal 8 ft × 8 ft (2.4 m × 2.4 m) opening of the metering chamber of the LSCS. The metering chamber walls are shown as dashed rectangles labeled M.C. in Fig. 2. The length of the test section in the side view exceeds that of the metering chamber. It extends directly out to the middle of the lower ledge of the Z-frame. Ordinarily, heat flow is symmetric with respect to vertical planes parallel to the walls of the metering chamber. For flat specimens which have no air space between the top of the metering chamber and the lower boundary surface of the test section, these planes of symmetry are planes of zero horizontal heat flux. The planes intersect the inside walls of the metering chamber for thin flat specimens and the half thickness of the walls for thick flat specimens.

As seen in the end view in Fig. 2, the manufactured home test section cannot be characterized as a flat specimen. There is a large air space between the top of the metering chamber walls and the ceiling of the test section. Metering chamber air circulates inside this space. It was included because two significant features of the construction of this test section impact thermal performance. These are the short (2.5 in. or 6.4 cm) heel (formed by the nominal 1 by 3 perimeter rail) and the extension of the ceiling over the wall's

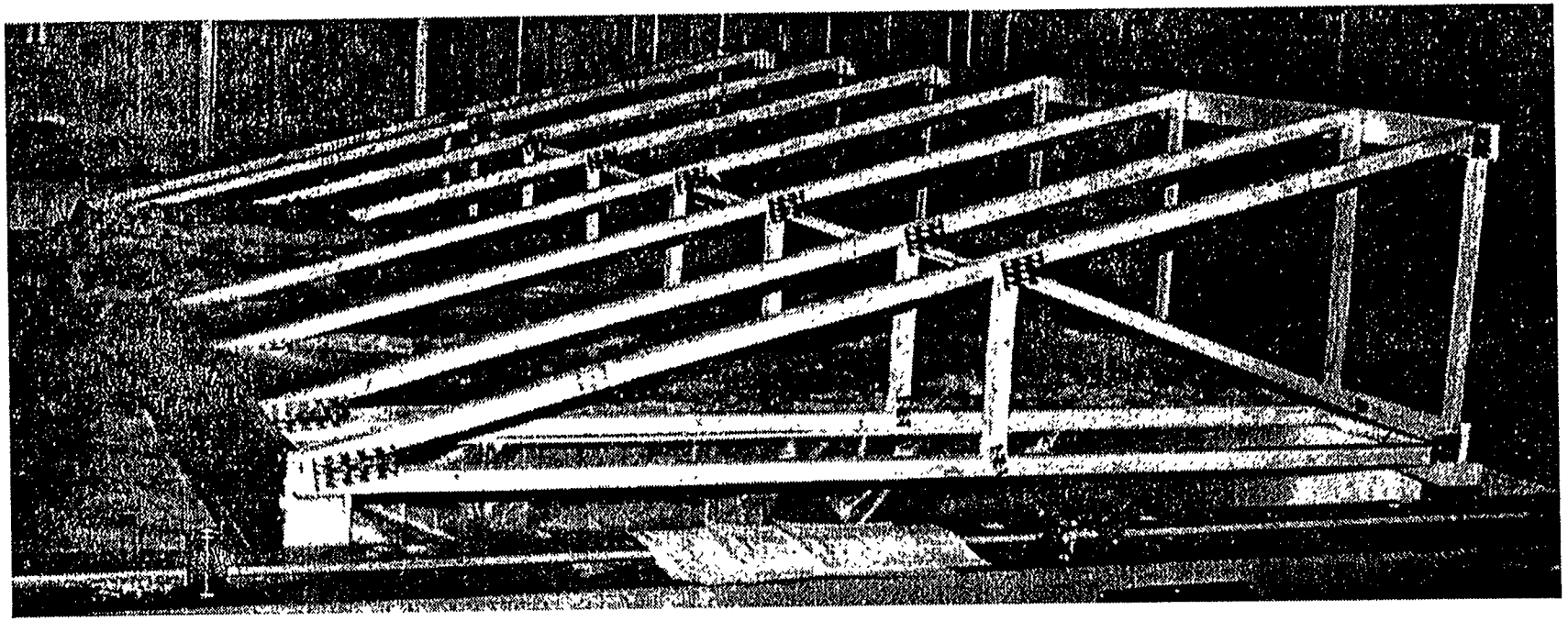

Fig. 1. Photograph of the manufactured home test section as built and before installation of instrumentation and guard insulation.

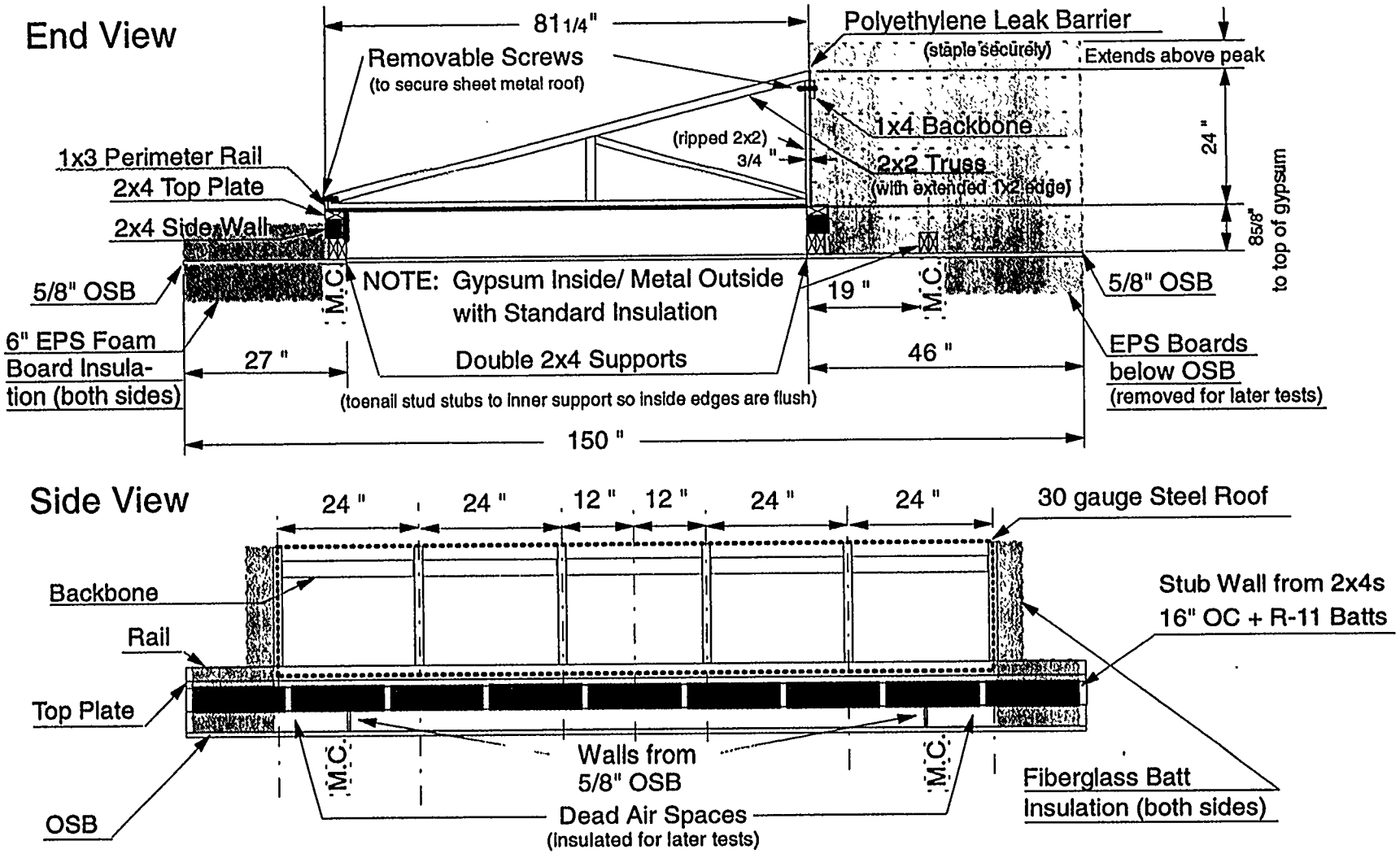

Fig. 2. End and side views of the manufactured home test section as built to fit into a Z-frame for a diagnostic platform in the Large Scale Climate Simulator.

top plate. There is little thermal protection along the eave edge of the ceiling from the reduced insulation in the vertical direction and the thermal bridge in the horizontal direction that these features cause.

To ensure that the full effect of this underprotected edge was measured calorimetrically and to allow testing of modifications, the test section was built on stub walls like the actual side walls of the unit whose features were incorporated in the design of the test section. These walls have drywall on the inside, aluminum siding on the outside and are filled with nominal R_{US}-11 (R_{SI}-1.9) fiberglass batt insulation between nominal 2 × 4 (actually 1.5 in. × 3.5 in. or 3.8 cm × 8.9 cm) studs located 16 in. (41 cm) on center (o.c.). There is a nominal 2 × 4 top plate. The thin gypsum board that forms the ceiling extended to the outside edge of the top plate in the assembly that was tested. It was covered by a piece of polyethylene which formed an air barrier/vapor retarder. Only 2.5 in. (6.4 cm) of side wall were exposed along the eave edge. The remaining 6.125 in. (15.6 cm) of the stub wall were hidden behind a slab of EPS insulation that guarded the eave edge. The slab of insulation rested on top of a 0.625-in. (1.6-cm) thick piece of oriented strand board (OSB) and both extended to the middle of the lower ledge of the Z-frame. The inside edge of the stub wall on the eave side lined up with the inside edge of the metering chamber wall.

As seen on the ridge side in the end view of Fig. 2, the half trusses were 19 in. (48 cm) short of reaching the other side of the metering chamber. Another stub wall with gypsum wallboard on its interior and its stud cavities filled with fiberglass batt insulation was built to support the ridge edges of the half trusses. A piece of OSB extended to the edge of the metering chamber and beyond to the middle of the edge of the Z-frame. For extra stiffness, two nominal 2 × 4 studs were placed side-by-side over the OSB where it rested on the metering chamber wall. The space over these extra studs and the exposed OSB was filled with EPS insulation boards that extended several inches above the peak of the trusses.

The total R-value of these EPS boards in the vertical direction, which is the direction of minimum thickness, is estimated to be 144 $h \cdot ft^2 \cdot °F/BTU$ (25.4 $m^2 \cdot K/W$). There is a small amount of heat flow through the horizontal OSB under the EPS into the metering chamber, which is not part of the heat flow for the roof. In standard guarded hot box techniques, a correction is made for heat flow between the guard and metering chambers by measuring the temperature difference across the known R-value of the metering chamber walls. This type of correction proved to be negligible because the differences between the guard and metering chamber temperatures were kept less than 0.5°F (0.3°C) on average. The same procedure was used to estimate the heat flow through the horizontal OSB from temperatures measured above the EPS and below the OSB. The correction amounted to about 2% of the total measured heat flow into the metering chamber.

Small heat leaks were also possible around the perimeter of the test section through vertical structural members indirectly exposed to the simulated outside conditions. Only the heat flow through the stub wall on the eave edge was part of the desired effect that the metering chamber energy balance measured. The other flanking losses besides the vertical heat flow through the R_{US}-144 EPS were estimated from the responses of thin, 2 in. × 2 in. (5.1 cm × 5.1 cm) heat-flux transducers (HFTs) in place around the perimeter. Along the length of the test section in the side view of Fig. 2, vertical walls of OSB

extended from the ceiling of the test section to the inside edges of the metering chamber walls. Caulking them prevented direct exchange of air between the guard and the metering chambers. Additional pieces of OSB extended horizontally from these walls to the middle of the edges of the Z-frame. Initially, only the multiple vertical pieces of unfaced fiberglass batt insulation shown in the lower part of the side view were in place. They allowed dead air spaces for 1 ft (0.30 m) outside both OSB walls. HFTs placed in the middle of the OSB walls monitored the average heat flux between the walls and the metering chamber. After enough measurements to include all the different climate chamber temperatures, each HFT was covered by a 6 in. (15 cm) square piece of 0.5 in. (1.3 cm) thick extruded polystyrene (XPS). Each HFT was calibrated facing a 2 ft (0.6 m) square piece of the same XPS to fit in a heat flow meter (ASTM 1991). The response of an HFT covered by XPS was applied to a unit area of bare wall by multiplying its indicated heat flux by the ratio of the thermal resistance of the wall plus the XPS and the wall only. The results checked with the data when the HFTs were not covered. The correction for each wall proved to be significant; about 4% of the measured total for the whole test section. To reduce this heat flow to about 2 to 3% of the total for each, these spaces were also filled with fiberglass batt insulation after the first two series of tests. A heat-flux transducer in the middle of the stub wall on the ridge side was used similarly. It showed a heat leak through the gypsum surface of about 2 to 3% of the total uncorrected flow.

A steady-state two-dimensional conduction heat transfer calculation was performed at all climate chamber temperatures to estimate the flanking losses horizontally through the wall and vertically through the OSB at the ridge edge. The 2-D calculation for the wall gave 0.9 to 1.0% of the total measured flow vs. 2.1 to 3.2% from the HFT. The 2-D calculation of the flanking loss in the vertical direction was 2.5 to 2.8% vs. 1.7 to 2.0% by the 1-D approach. The results from the HFTs on all three walls and the 1-D estimate for the vertical flow through the OSB on the ridge edge were used to correct the energy balance.

Even though the total energy flow into or out of the metering chamber is corrected for flanking losses, it is important to minimize the losses. Techniques to measure components of the flanking losses are judged accurate to about ±10%. If individual flanking losses are less than 5% of the total, each one affects the accuracy of the total by less than ±0.5%. Besides minimizing the flanking losses, the guard insulation reduced the thermal load on the guard chamber around the metering chamber. More importantly, it prevented relatively cold or hot spots around the perimeter of the metering chamber from generating significant heat flow between the metering chamber and the guard chamber. This was also the rationale for initially trying the slabs of foam insulation shown in the end view of Fig. 2 below the test section outside the metering chamber.

The vertical pieces of fiberglass insulation shown on the upper part of the side view in Fig. 2 were kraft paper faced. They sealed the ends of the attic space to prevent air flow along it except that from natural convection currents inside it. Polyethylene was stapled over the ends of the half trusses at the ridge edge also to seal the attic from air leakage. In the measurements with blown-in rock wool, polyethylene was stapled and taped to the two trusses just beyond the metering chamber and a 16 in. (41 cm) thickness of fiberglass batt insulation was wedged against them. The polyethylene provided an additional air seal

and prevented the rock wool from spilling out of the test section. The extra insulation minimized heat flow into or out of the attic space through the gable ends when insulation over the trusses replaced the metal roof.

The nominal R_{US}-7 fiberglass batts used inside the attic space in Configurations A, B and C were 24 in. (61 cm) wide and 2.25 in. (5.7 cm) thick when expanded. This matches the thickness on the insulation package label. They were cut to the length from eave edge to ridge inside the attic. The bulk density of two typical pieces was determined to be 0.53 lb/ft^3 (8.5 kg/m^3). The first layer for all configurations was easily forced between the ceiling joists. The pieces for the second layer in the two-layer fiberglass batt configuration were laid over the first layer in the same direction and butted closely against their neighbors except where vertical and slanted trusses were joined to the joists. The gaps persisted beyond the actual location of vertical and slanted trusses due to semi-rigidity of the batts. The second layer was removed for the tests with the PEP insulation. Figure 3 shows the PEP insulation in place in the test section; compare it to the view shown in Fig. 1. The PEPs that were made available by a German manufacturer for the tests were approximately 0.79 in. (20 mm) thick, 30 in. (76 cm) long, and wide enough (about 22.5 in. or 57 cm) to fit snugly between the 24 in. (62 cm) o.c. nominal 2 × 2 joists, but could not butt against their neighbors in adjoining spaces between joists because of the trusses. The top of each PEP, as seen in Fig. 3, was a heavy foil sheet. The perimeter of each panel consisted of a thin strip of the foil about 0.5 in. (1.3 cm) wide, which was sealed to the edges of the shallow plastic container for the silica powder material that formed the 20 mm thick body of the panel. The panel nearest the eave edge in each space between joists rested with one of its narrow edges on the perimeter rail. The narrow end of the middle panel overlapped those of its neighbors in the same joist space. The third panel extended about six inches (15 cm) beyond the ridge edge through a slit in the polyethylene barrier placed over the ridge edge (see Fig. 2). The extension rested in a slot cut out of the EPS foam boards on the ridge edge and was chinked with fiberglass.

Figure 4 shows the three layers of fiberglass batts that were placed on the ceiling as part of Configuration C. Not shown in the figure is the fourth layer of fiberglass batts that completed the configuration. The batts for this layer had the same thickness as the others but were wide enough so two strips covered the entire area over the roof trusses. Wide tape held them together and they stayed in place when the roof was rolled back over the trusses. This layer is called a rumble blanket because it prevents the metal roof for manufactured homes from rattling in the wind.

For additional comparison of the insulation configurations and to emphasize the naming convention for them used in this report, see Fig. 5. Note the air spaces that are shown over the ceiling joists in the three Configurations A, B and C with fiberglass batts. They were created by the force fit of layers of fiberglass batt insulation between the ceiling joists. Like the gaps between batts beyond the places where the vertical and slanted truss members joined the joists, these spaces were not present when the blown-in rock wool insulation of Configuration D was used instead of batts. Blown-in insulation fills in such gaps and spaces when it covers the ceiling joists completely as it did here. The average thickness of the blown-in rock wool was 4.1 in. (10.4 cm) compared to the 1.5 in. (3.8 cm) high joists.

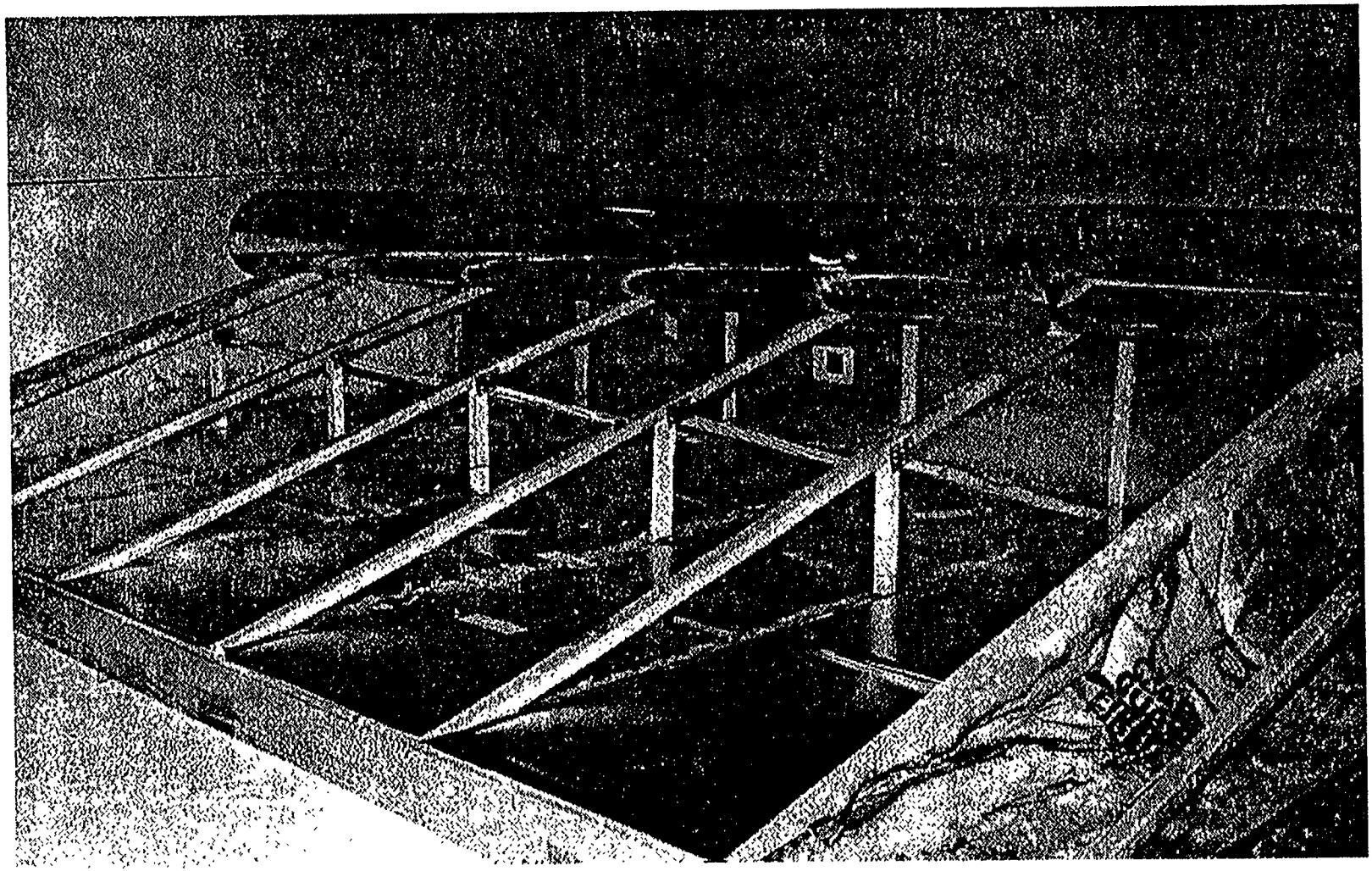

Fig. 3. Photograph of the manufactured home test section after installation of instrumentation and guard insulation and with PEPs in place over a single layer of fiberglass batts on the ceiling.

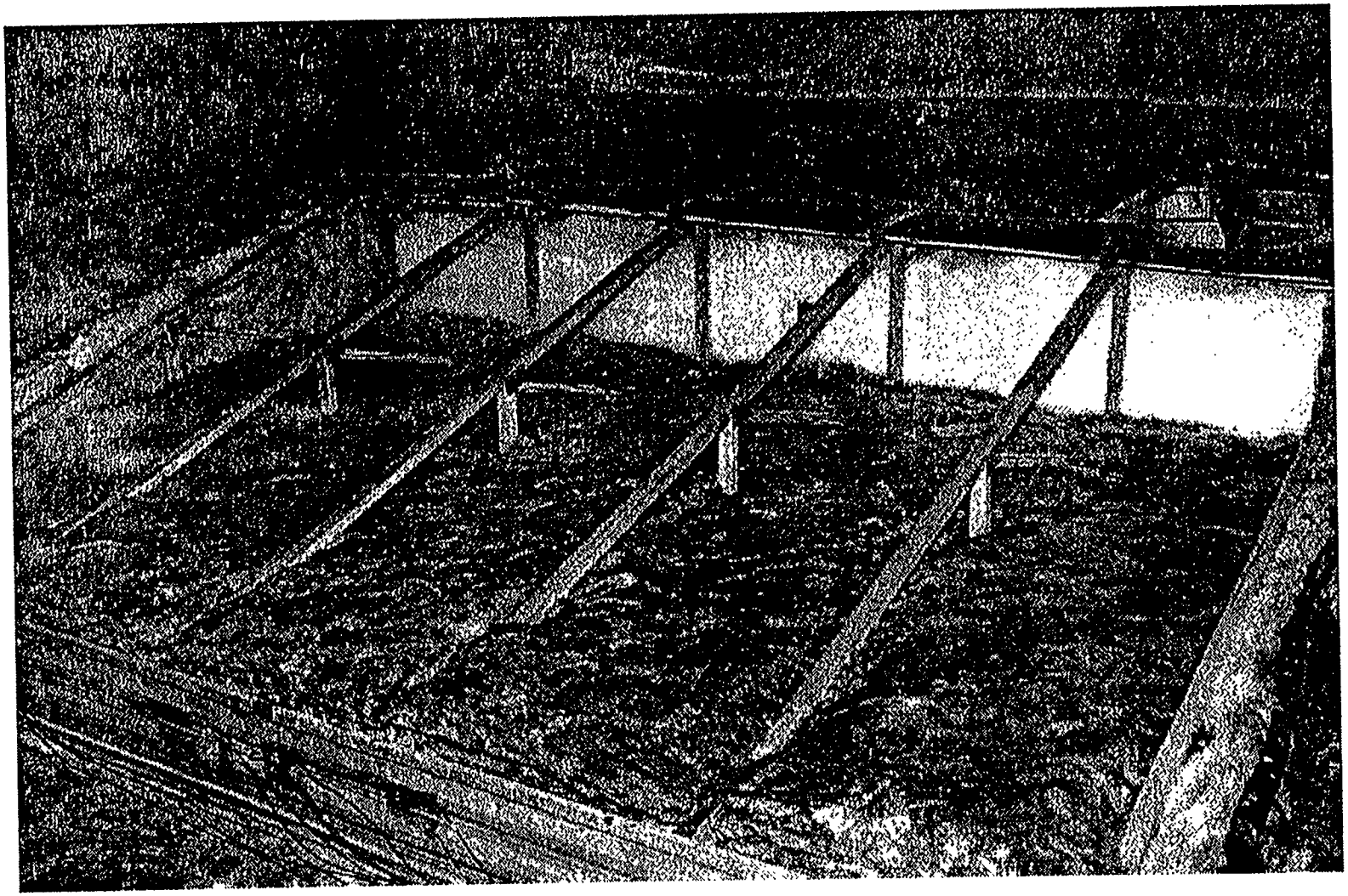

Fig. 4. Photograph of the manufactured home test section with three layers of fiberglass batt insulation installed on top of the ceiling.

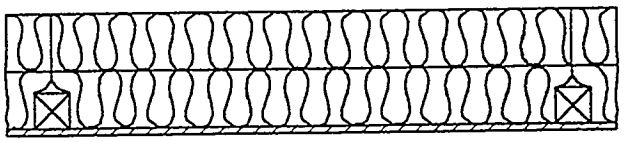

A. Two layers of fiberglass batt insulation on top of the ceiling.

B. Powder-filled evacuated panels (PEPs) on top of a layer of fiberglass batt insulation.

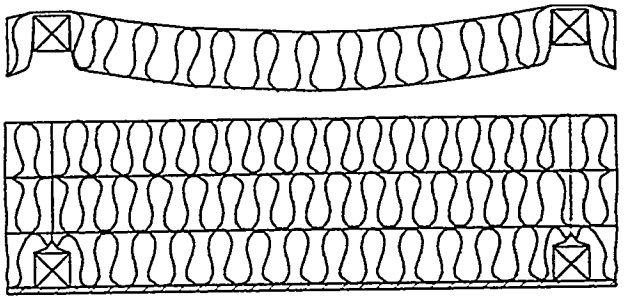

C. Three layers of fiberglass batt insulation on top of the ceiling and a rumble blanket on top of the slanted roof trusses.

D. Blown-in rock wool insulation at an average thickness of 4.1 in. (10.4 cm).

Fig. 5. Cross-sections of insulation Configurations A, B, C and D shown to scale between nominal 2 in. × 2 in. (actual 3.8 cm × 3.8 cm) horizontal ceiling joists 24 in. (0.61 m) o.c. away from the vertical and slanted truss members.

3. INSTRUMENTATION IN THE TEST SECTION AND PROCEDURES

The manufactured home test section was equipped with 97 copper-constantan thermocouples to supplement the thermocouples built into the upper and lower chambers of the LSCS for control and monitoring purposes. Figure 6 shows the end and side views of the test section but without the dimensions and other details in Fig. 2. Instead, the location of instrumentation is presented for the configuration with two fiberglass batts. The batts are represented by the dashed lines on top of the gypsum ceiling in both views. Six thermocouples were placed in the air directly under the ceiling to see how well the temperatures they indicated matched those measured by the 20-member array of thermocouples in a horizontal plane near the top of the metering chamber. Another 23 measured the temperature of the surfaces inside the ceiling space above the plane of the top of the metering chamber. Eight thermocouples were used to check the horizontal OSB temperatures and ensure that the temperatures outside the metered area were not different enough from the metering chamber temperature to allow significant heat flow along the OSB. Pairs provided temperature differences ΔT and were placed on the underside of the OSB on each of the four sides. On the eave side, the pair was $\Delta x = 8.5$ in. (22 cm) apart; on the ridge side, 25 in. (64 cm) apart; and, on the two ends, 13.5 in. (34 cm) apart. The gradients $\Delta T/\Delta x$ were multiplied by the thermal conductivity of OSB and by the cross sectional area perpendicular to Δx to estimate the heat flow along each OSB extension into the metering chamber. The amounts were negligible compared to the measured total heat flow. There were 25 thermocouples to measure gypsum, joist and insulation surface temperatures inside the attic space. The roof and aluminum siding temperatures were monitored by 23 thermocouples attached to the outside surfaces of the test section. The remaining 12 thermocouples were for air temperatures directly above the test section.

To provide insight to the measurements, computer modeling was part of the data analysis. Several temperatures near the eave edge were measured specifically to validate the model of the edge. The ceiling and inside eave wall surfaces in the mid-plane of the test section in the side view of Fig. 6 were instrumented with five thermocouples, one at the inside corner and the others at 1.5 in. and 3.0 in. (3.0 cm and 7.6 cm) from the corner both horizontally and vertically. Six thermocouples were located outside the test section on the aluminum siding at the level of or below the top plate. There were also two thermocouples inside the attic space at the location where the top of the gypsum ceiling met the perimeter rail that formed the heel. Averages were taken for the outside and attic edge temperatures.

The lead wires for the thermocouples that measured air temperatures both above and below the test section were led along the respective surfaces and were bent at a 90° angle to the surface about 3 in. (7.6 cm) from their measuring junctions to form unshielded air temperature probes. Lead wires for thermocouples to measure surface temperatures were lain along the surfaces in a direction judged to be isothermal with the point of interest. The bead itself was taped to the surface with masking tape at the desired location. If the surface was shiny metal, aluminum tape was used over the masking tape to match reflectance. To keep the thermocouples in place on nonmetallic surfaces, staples were used to pin down the lead wires without compromising their electrical insulation.

End View

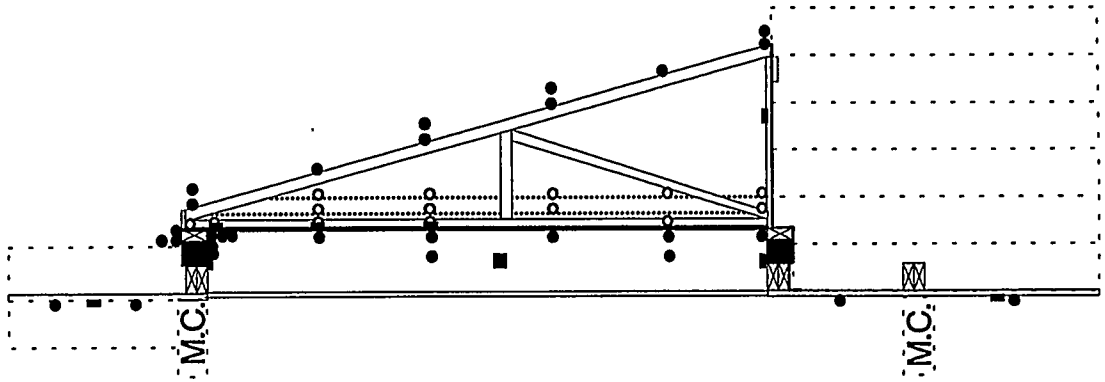

Legend:

- o Thermocouple inside Attic Space
- • Thermocouple outside Attic Space
- ■ Heat-Flux Transducer

Side View

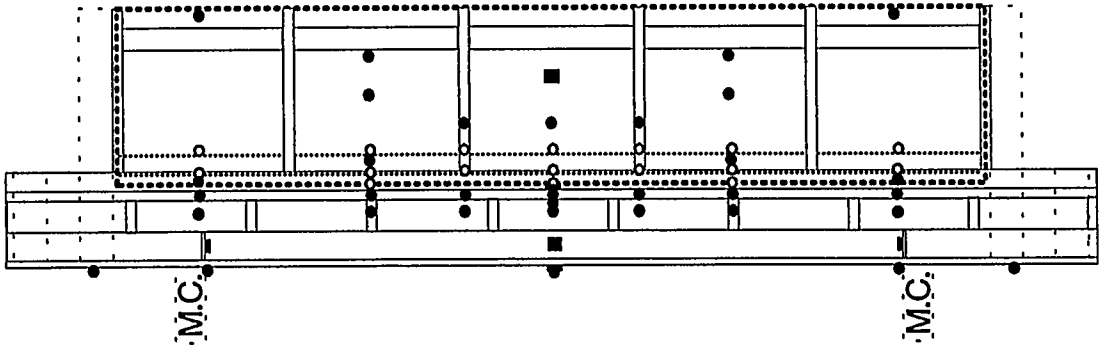

Fig. 6. End and side views of the manufactured home test section to show the location of thermocouples and heat-flux transducers for the configuration using two layers of fiberglass batts.

The total heat flow through the test section was determined calorimetrically by an energy balance on the metering chamber. Checks of the accuracy of the balance were performed as part of the tests. A calibration panel, comprising a 4 in. (10.2 cm) thick layer of EPS with R-value known as a function of temperature, was inserted into the LSCS. The metering chamber balance reproduced the panel's R-value of about 16 h·ft²·°F/BTU (2.8 m²·K/W) within ±0.1 h·ft²·°F/BTU (±0.02 m²·K/W) at mean insulation temperatures from 25 to 50°F (-4 to 10°C). Auxiliary heating was required to maintain a constant temperature in the metering chamber under these conditions. This is called guarded hot box operation. At summer conditions, cooling of the metering chamber was required to hold steady-state. This is called guarded cold box operation. A special cooling loop was used to overcool the metering chamber so its temperature could be controlled with heaters just like in guarded hot box operation. For optimum cooling, which was determined empirically, R-values for the calibration panel were within ±0.3 h·ft²·°F/BTU (±0.06 m²·K/W) of known values at mean insulation temperatures from 85 to 100°F (29 to 38°C). The success of these accuracy checks indicates that there is no significant systematic error in the energy balances on the metering chamber, since the operating conditions in all chambers were varied over the same ranges and in the same manner for the calibration panel and the manufactured home test section.

In addition to the local heat fluxes from calibrated HFTs that were used to correct the total heat flow for flanking losses over the end walls and the ridge wall, several other local heat fluxes were monitored by HFTs placed as in Fig. 6. Three HFTs were used to monitor how close the heat flux was to zero around the perimeter of the test section where there was no direct exposure to the metering chamber. They were checked for behavior near zero heat flux by observing their steady-state response while held between two 1 in. (2.5 cm) thick pieces of EPS on a workbench at room temperature. Two were installed by taping them underneath the horizontal OSB outside the metering chamber. The slabs of EPS insulation shown in Fig. 2 outside the metering chamber underneath the test section on the eave and ridge sides were pushed against these HFTs in early tests, but later the EPS was removed to minimize heat leaks into the metering chamber. With the boards in place, vertical heat fluxes into the guard chamber indicated by these HFTs were low. However, the thermocouples there indicated that significant heat flow along the OSB into the metering chamber was possible. There was more heat load on the guard chamber without this insulation, but the temperature of the OSB was close to the guard chamber temperature and heat flow along the OSB into the metering chamber was negligible. The third HFT was taped to the outside of the polyethylene in the middle of the ridge side of the attic space. The EPS that guarded the ridge side of the test section was shoved against it. It showed small heat flux during all the tests.

Three more HFTs were especially calibrated for use inside the attic space of the manufactured home test section. During calibration, they were taped to gypsum board and covered by two layers of the nominal R_{US}-7 fiberglass batt insulation or the rock wool used for the base-case insulation configurations. For all the tests, these three HFTs were taped in place on the top of the ceiling in the middle space of the five spaces between trusses at varying distances out from the eave edge. In the first few tests with the two layers of fiberglass batts, one HFT was placed against the perimeter rail while the other two were placed about 0.4 and 0.8 of the distance from the rail to the ridge edge along the top of the gypsum. The latter two sensors gave essentially identical results while the one at the edge yielded confusing data.

Thermocouples on the ceiling near the edge HFT suggested a large horizontal temperature gradient at the location so that the heat flow had a significant horizontal component. Calibration of the HFTs was done with a uniform temperature above and below them to yield a calibration constant for vertical heat flux only.

For the rest of the tests, the HFT closest to the edge (designated HFT 1) was moved so its center was 3.75 in. (9.5 cm) from the inside of the perimeter rail, that is, just beyond the edge of the nominal 2 × 4 top plate. For the other tests with a layer of fiberglass over the ceiling, another (designated HFT 2) was located with its center at 13.75 in. (34.9 cm) from the inside of the perimeter rail, that is, a few inches beyond the end of the region in which the roof atop the trusses compressed the two layers of fiberglass batts comprising Configuration A. For the rock wool tests, HFT 2 was moved so that its center was 8 in. (20 cm) from the inside of the perimeter rail. This was where the rock wool was at half the eave edge thickness. For all tests except the few at the beginning, the center of the third (designated HFT 3) was located 35.75 in. (90.8 cm) from the inside of the perimeter rail. At this location all configurations, even Configuration C, had enough room to expand.

As seen in Fig. 6, thermocouples were located beside each HFT inside the attic space at the same distance from the perimeter rail as the center of their respective HFTs. To yield a temperature difference, thermocouples were also located directly above HFTs 2 and 3 on top of the insulation. Roof temperature was used for HFT 1. This placement of HFTs and thermocouples gave data to estimate center-of-cavity R-values of the insulation configurations and apparent insulation R-values near the eave edge of the test section.

The initial tests with the manufactured home test section used two layers of fiberglass batt insulation on top of the gypsum ceiling between the ceiling joists and trusses. In these tests, HFTs 2 and 3 were approximately 0.4 and 0.8 of the distance from the inside edge of the perimeter rail to the peak, respectively, in the middle of the space between the centermost joists. Thus, both of them were covered by two expanded fiberglass batts. According to the label information on the insulation package, the nominal (at 75°F or 24°C) R-value of one batt is R_{US}-7 (R_{SI}-1.2) at a thickness of 2.25 in. (5.7. cm), which was the observed thickness. Fig. 7 shows R-values as a function of mean insulation temperature. The R-values from HFTs 2 and 3 are computed from $\Delta T/q$, where ΔT is the difference in temperatures indicated by the thermocouples on top of the insulation and beside each HFT and q is the measured heat flux. R-values from HFTs 2 and 3 for tests at winter conditions and a summer condition are plotted. The mean temperatures of the insulation are the averages of the thermocouple readings used for the ΔTs.

The solid line in Fig. 7 is from a correlation by Wilkes (1979) for the R-value of fiberglass batt insulation that is L = 4.5 in. (11.4 cm) thick with area A = 1 ft² (0.093 m²) and nominal density ρ_{nom} = 0.624 lb/ft³ (10.0 kg/m³). In equation form,

$$R = \frac{L}{kA} \quad with \quad k_{75°F} = 0.19815 + 0.001573 \cdot \rho/\rho_{nom} + 0.11686 \cdot \rho_{nom}/\rho$$

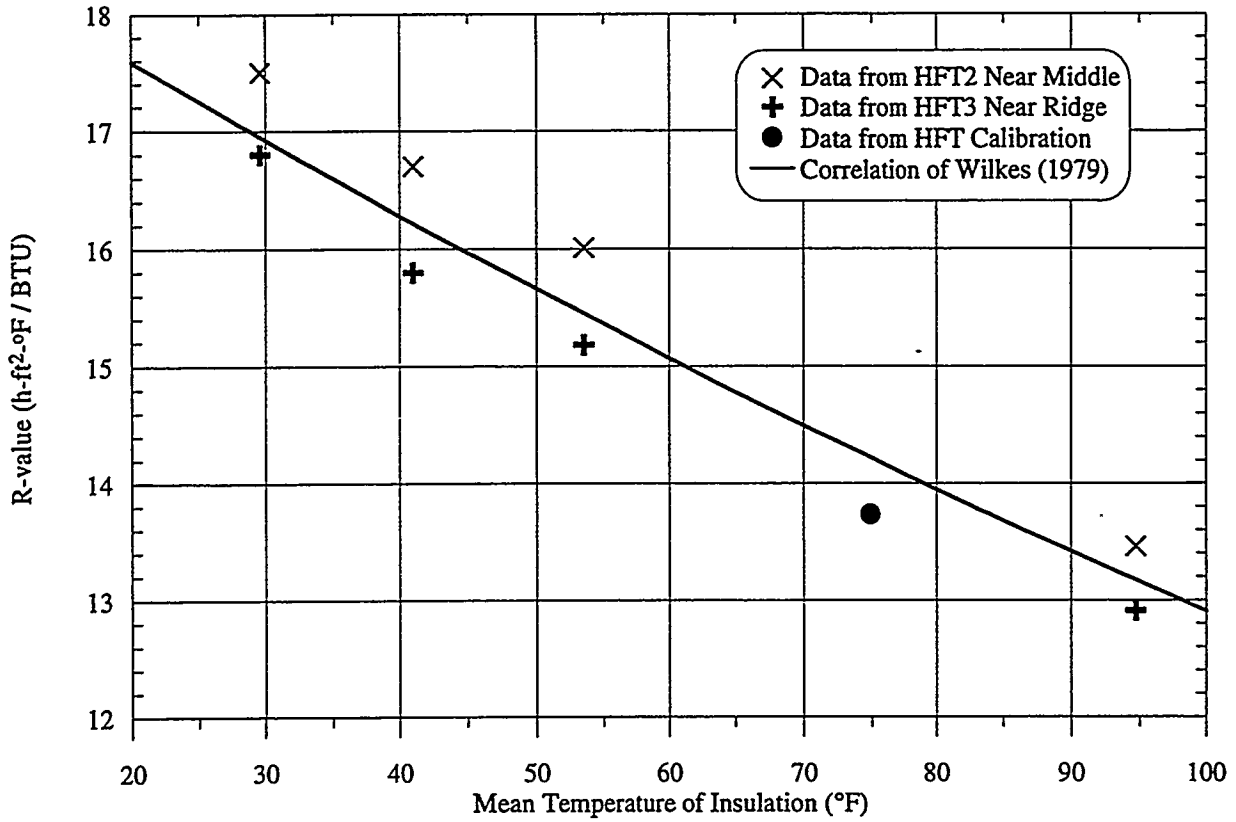

Fig. 7. Results from the heat-flux transducers HFTs 2 and 3 in tests at winter conditions and a summer condition compared to a correlation by Wilkes and data obtained during calibration of HFTs 1, 2 and 3.

$$and \quad k_T = k_{75°F}\, exp[(0.0020201 + 0.0018486 \cdot \rho_{nom}/\rho) \cdot (T - 75)] \qquad (1)$$

where R is the R-value in h·ft²·°F/BTU,
L is the thickness in inches,
A is the area in ft²,
k is the thermal conductivity in BTU·in./(h·ft²·°F),
ρ is the density in lb/ft³, and
T is the temperature in °F.

Equation (1) best fits the data in Fig. 7 with density $\rho = \rho_{nom} = 0.624$ lb/ft³ (10.0 kg/m³). It is used throughout this report to calculate the R-value of fiberglass batts as a function of temperature and density. We measured density $\rho = 0.53$ lb/ft³ (8.5 kg/m³) for the fiberglass batts used in the experiments. The density difference is attributed to a difference in fiber diameters. With nominal thermal conductivity k_{nom} = 0.32 BTU·in./(h·ft²·°F) [0.046 W/(m·K)] at 75°F (24°C), the ASHRAE Handbook of Fundamentals gives diameter of about 20×10^{-5} in. (0.005 mm) at $\rho = 0.53$ lb/ft³ and diameter of about 28×10^{-5} in. (0.007 mm) at $\rho = 0.624$ lb/ft³ (ASHRAE 1993). The smaller fiber diameter is more typical of current fiberglass batts; the larger fiber diameter is typical of fiberglass batts described by Eq. (1) (Wilkes 1995).

The additional point at 75°F (24°C) in Fig. 7 is the R-value of a specimen of two layers of the same fiberglass batts as were used to insulate the ceiling cavity of the test section. The specimen was cut in the shape of a 2 ft (0.61 m) square for use in a heat flow meter operated in accordance with ASTM C 518 (ASTM 1991) to calibrate HFTs 1, 2 and 3. HFTs 2 and 3, along with the respective temperature differences, yielded R-values that agree within ±0.4 h·ft²·°F/BTU (±0.07 m²·K/W) of the correlation. This uncertainty corresponds to a ±0.125-in. (±0.32-cm) uncertainty in the thickness of the fiberglass batts. Spot checks with a ruler for a batt of the fiberglass laid on the laboratory floor showed this much variation in its thickness. The correlation, in turn, agrees within the same error with the data from heat fluxes and temperature differences between the plates of the heat flow meter during HFT calibrations.

The agreement in Fig. 7 among the R-values using the HFTs and the heat flow meter is assurance that the heat-flux transducers and thermocouples in the test section produced accurate data for the center-of-cavity R-values with acceptable scatter from HFT to HFT. In the spreadsheets used for data analysis, working graphs and inspection of the maximum, minimum, average and standard deviation of results over the time range for steady-state at each set of imposed conditions were used to assure accurate data and to estimate the precision of the data.

To check the behavior with increasing density of the fiberglass batts used in the tests against Eq. (1), data were obtained for two batts at 75°F (24°C) and no compression, 10% compression and 20% compression in accordance with ASTM C 653 (ASTM 1992a). These data and an additional point at 75% compression are shown in Fig. 8. The solid line shows the behavior of Eq. (1) at 75°F (24°C) over the range of ρ/ρ_{nom} needed to predict compression effects at the edge of the test section. The dashed curve fits the points at no compression and 20% compression and is forced to have a minimum at $\rho = 2$ lb/ft³ (32 kg/m³), which is the density for a minimum observed by Desjarlais *et al.* (1980). The additional point measured at high density agrees with the dashed curve. Using Eq. (1) to predict the effect of compression gives thermal conductivities that are higher than the dashed curve by at most 10% of k_{nom} over the range shown in Fig. 8. Equation (1) is based on data for many samples of fiberglass batts albeit ones older than the fiberglass batts used in these tests.

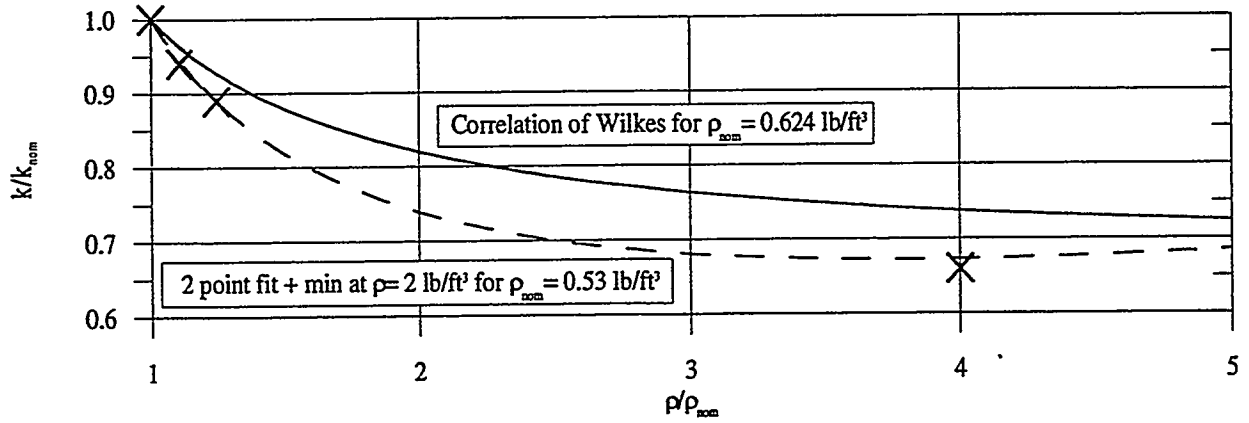

Fig. 8. Comparison of the effect of increased density in the correlation of Wilkes at ρ_{nom} = 0.624 lb/ft³ to data for the fiberglass batts with ρ_{nom} = 0.53 lb/ft³ used in the tests.

4. RESULTS OF TESTS AND DISCUSSION

4.1. TESTS WITH THE TWO-LAYER FIBERGLASS BATT CONFIGURATION AND WITH PEPS ON TOP OF FIBERGLASS BATTS (CONFIGURATIONS A AND B)

A listing of the sets of temperatures imposed during the tests is shown in Table 1. Names for the tests start with W1, W2, W3 or S2. An "A", "B", "C" or "D" suffix is added to designate the insulation configuration of Fig. 5. An "r" suffix denotes a repeated run at conditions and insulation configuration identical to a run without the "r" suffix. An "x" suffix means an extended run with new insulation features such as additional sheathing. The order of tests with the two layers of fiberglass batts was W2A, W1A, W3A, W1Ar, S2A, W2Ar and S2Ar. The repeated run W1Ar was done between W3A and S2A to check reproducibility. The location of the HFTs was then changed and the repeat test, W2Ar, was done after S2A as a check before installing the PEPs as a replacement for one layer of fiberglass batts. S2Ar was done several months later after a new cooling loop was installed in the metering chamber. The order for the runs with the PEPs on top of a layer of fiberglass batts was W2B, W3B, W1B, W1Br and W2Bx. W1B and W1Br were the runs just before and immediately after the empty space next to the OSB walls and over the guard chamber was filled with fiberglass batt insulation. The latter verified that less heat was flowing between the climate and metering chambers after these walls were insulated.

Table 1. Temperatures imposed in the chambers of the Large Scale Climate Simulator for tests with the manufactured home test section

Winter	Climate Chamber	Metering and Guard Chambers
W1	25°F (-4°C)	75°F (24°C)
W2	0°F (-18°C)	75°F (24°C)
W3	-25°F (-32°C)	75°F (24°C)
Summer	**Climate Chamber**	**Metering and Guard Chambers**
S2	125°F (52°C)	75°F (24°C)

Figure 9 shows the comparison between the center-of-cavity R-values for Configuration A, using the averages of the data from HFT 2 and HFT 3, and Configuration B with PEPs, using data from HFT 2 only. Center of cavity means well away from any effects at the joints between the PEPs or effects at the joists for both systems. HFT 3 was near a joint between PEPs. The mean temperatures of the two configurations were slightly different despite nominally identical chamber conditions. The differences between the center-of-cavity R-values for the fiberglass batt and PEP (Configuration B) and half the values for the two fiberglass batts (Configuration A) were taken at the three sets of almost equal mean temperatures. The layer of fiberglass was compressed about 0.125 in. (0.32 cm) under the PEP, which is heavier than another layer of fiberglass. The effect on R-value of this compression was ignored. The solid curve drawn on Fig. 9 approximates the R-value of the PEP alone, which has a thickness of about 0.79 in. (2.0 cm). It is thermally equivalent to two layers of fiberglass batts with an expanded thickness of 4.5 in.

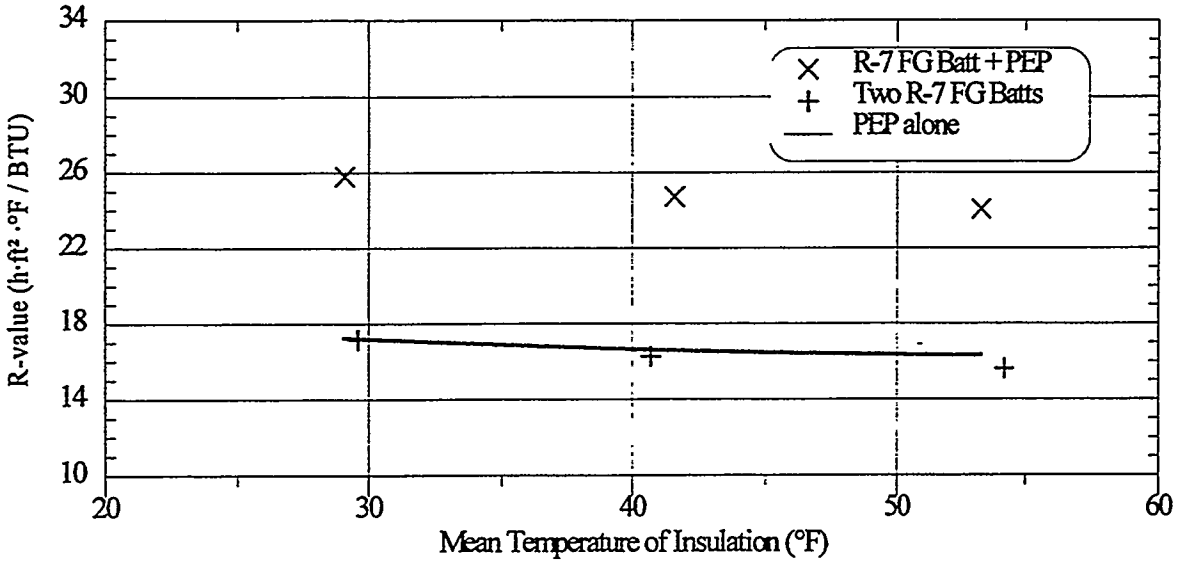

Fig. 9. Comparison of R-values for the fiberglass batt insulation and PEPs in tests at winter conditions.

(11.4 cm). The minimal temperature dependence shown by the R-value of the PEP allows an estimate for its nominal (75°F or 24°C) value: about R_{US}-16 (R_{SI}-2.8) or R_{US}-20 per inch (R_{SI}-1.4 per cm).

An energy balance on the metering chamber of the LSCS is used to calculate an R-value for the system. For these tests, it is defined as

$$R_{system} = \Delta T \cdot A/Q \qquad (2)$$

where ΔT is the difference between the average air temperatures above and below the test section,
A is the inside surface area of the test section exposed to the metering chamber, and
Q is the net heat flow through this area.

Because a correction is made for heat flow through the insulated surfaces around the perimeter of the test section, the area is simply taken as the sum of the ceiling area and the area of the stub wall above the EPS insulation on the eave side. The ceiling area is 96 in. × 76.25 in. (2.44 m × 1.94 m) and the exposed stub wall area is 96 in. × 2.5 in. (2.44 m × 0.064 m), totaling 52.5 ft² (4.89 m²). The stub wall contributes only 3.2% to the total area.

The stub wall is insulated with nominal R_{US}-11 fiberglass batt insulation. If there were neither any effects of joints, joists and studs nor any effects of the thermal bridge or reduced insulation R-value at the edge of the test section, the effective R-value of the insulation would be given by

$$A/R_{eff} = A_{ceiling}/R_{ceiling} + A_{wall}/R_{wall} \qquad (3)$$

where the wall area A_{wall} is small compared to the ceiling area $A_{ceiling}$. In this one-dimensional, parallel path approach, in U.S. units, R_{eff} = 15.8 if $R_{ceiling}$ = 16 (Configuration A), and R_{eff} = 23.1 if $R_{ceiling}$ = 24 (Configuration B), due to the small wall area. Besides neglecting thermal shorts, these estimates of the

and bordering any spaces where insulation does not touch the roof. For summer conditions, radiant barrier effects due to the metal roof (with an estimated reflectance of 0.77) are discussed later in the section on results with the blown-in rock wool insulation, but do not affect the rough estimates with Eq. (3). The thermal bridge horizontally at the eave, the reduced insulation R-value vertically at the eave edge (due to lack of room for insulation or compression effects) and the difficulty of insulating near the trusses contribute to a reduction of the system R-value below the center-of-cavity R-value over the ceiling.

Figure 10 shows the system R-values, obtained from measured temperatures and the metering chamber heat flow corrected using Eq. (2), and compares them to center-of-cavity R-values. The two-layer fiberglass batt system, Configuration A, allows effects of both compressed insulation and the thermal bridge at the eave edge. There are also effects of the gaps where the second layers of fiberglass could not butt against each other due to interference by the slanted and vertical truss members. The system R-values average 12.2 and show no significant temperature dependence. They are 72 to 77% of the center-of-cavity R-values at the winter conditions. The summer value is 92% of the corresponding center-of-cavity value due, we believe, to a radiant barrier effect of the metal roof.

Configuration B is subject to the effects of the horizontal thermal bridge at the edge, but the insulation at the edge is not compressed like in Configuration A. Because the PEPs did not cover the top of the ceiling joists while the second layer of the fiberglass batts did, the effects due to lack of insulation over the joists are likely more severe for the superinsulation configuration. There are also two joints between PEPs in each space along the span from eave to ridge. The net result is a slight increase in system R-value to an average of 12.6 compared to 12.2 for the two layers of fiberglass batts. The system R-value is 49 to 53% of the higher center-of-cavity R-value for the PEPs at winter conditions. PEPs were not tested at summer conditions.

The 95% confidence interval for the system R-values with both Configurations A and B is ±0.5 h·ft²·°F/BTU (±0.09 m²·K/W) from twice the typical standard deviation of the R-values measured over the steady portion of each test. For measurements with uncertainties due to systematic errors, u_S, and due to precision errors, u_P, overall uncertainty is $u_M = (u_S^2 + u_P^2)^{½}$ (Coleman 1989). In the absence of significant systematic errors in the metering chamber energy balance, the flanking losses, temperatures across the test section and the area of the test section, u_M reduces to u_P. Precision error can be estimated as Student's test statistic multiplied by the standard deviation of the average. Data for the averages were recorded every four minutes for at least 12 hours of steady-state operation. Thus, Student's test statistic for 95% confidence has the value 2. The R-value for the PEP system is largest at its highest mean insulation temperature. Since the value is within the confidence interval about the average of the system R-values, it is likely due to scatter rather than an indication of the system's temperature behavior.

The reason why the PEP system does not show a significant improvement in system R-value was postulated to be effects at the eave edge and over the joists and joints. Run W2Bx was done to test the hypothesis. Figure 11 shows a photograph of measures taken for this run to improve the insulation coverage over the joists and joints. EPS blocks were sawed to a 4 in. × 4 in. (10 cm × 10 cm) cross-section, cut to the length between vertical truss members and tapered to fit under the slanting truss members. Other lengths were cut to fit crosswise over the joints between PEPs. Strips of R_{US}-7 fiberglass were installed under the EPS blocks and all joists and joints were covered snugly. To lessen the edge

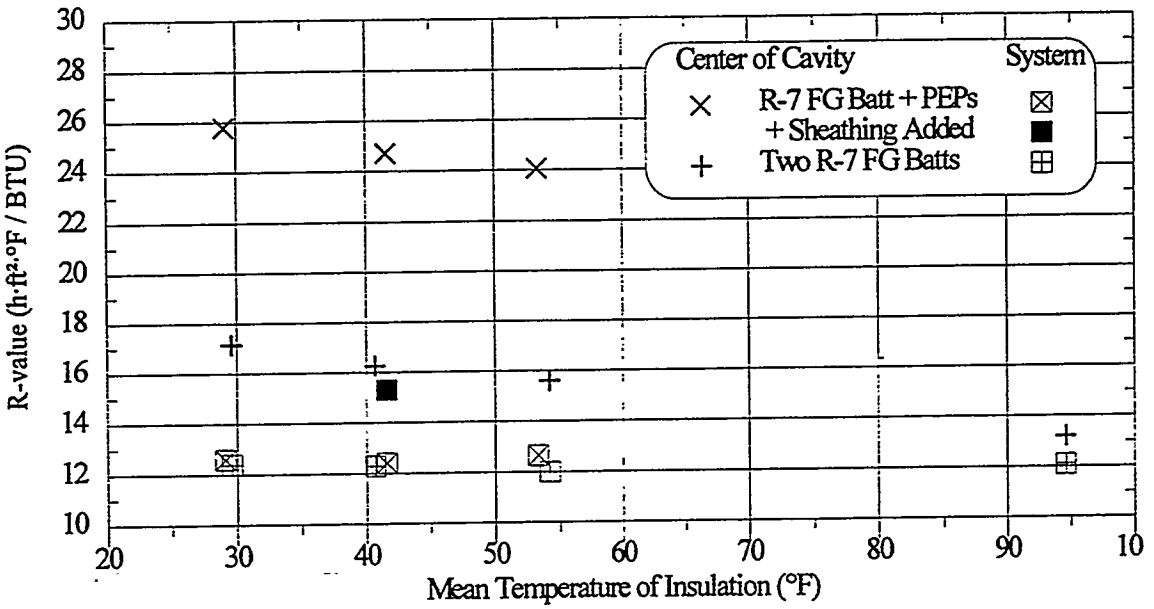

Fig. 10. Comparison of the R-values across the center-of-cavity insulation with the system R-values for Configurations A and B.

effects, pieces of 0.75 in. (1.9 cm) thick XPS sheathing were cut to cover the edge of the test section under the aluminum siding. Other pieces were placed on top of the trusses from the edge to about 20 in. (51 cm) from it. When steady-state conditions were achieved for Run W2Bx, the system R-value was R_{US}-15.3 (R_{SI}-2.7), 23% better than the original R_{US}-12.4 in W2B. The solid square in Fig. 10 shows this result. The run continued after data for this result were obtained. The pieces of XPS sheathing atop the trusses were removed for the continuation. Steady-state conditions yielded R_{US}-14.9 (R_{SI}-2.6); that is, 3.2% out of the 23% improvement was due to covering the trusses with XPS. This is a relatively small effect which confirms that the PEPs do a good job of insulating the eave edge of the test section vertically. More discussion of this feature is presented in overall comparisons of the configurations with fiberglass batts after the following discussion of results with Configuration C.

4.2. TESTS WITH FOUR LAYERS OF FIBERGLASS BATTS (CONFIGURATION C)

For the series of tests with Configuration C, tests designated W2C, W3C, W1C, S2C and W2Cr were done without the extra vertical XPS sheathing at the edge. W2Cr followed S2C to check reproducibility in case the summer conditions had caused moisture to collect at the bottom of the roof cavity. The extra edge sheathing was replaced for Run W2Cx. It was removed again for S2Cr, done several months later after a new cooling loop for the metering chamber was installed. For all the tests in this series, the fourth layer of fiberglass batts placed on top of the trusses allowed another nominal R_{US}-7 layer of insulation between trusses. Over the trusses themselves, however, it was compressed to a thickness of about 0.25 in. (0.64 cm). Using Eq. (1), its R-value at this thickness is estimated to be only R_{US}-1.2 (R_{SI}-0.21) at 40°F (4°C), a typical mean temperature of the insulation in these tests. Nonetheless, the compressed insulation does provide a break in the thermal bridge through the trusses especially near the eave edge where the roof trusses and ceiling joists are joined by metal plates (see Fig. 1).

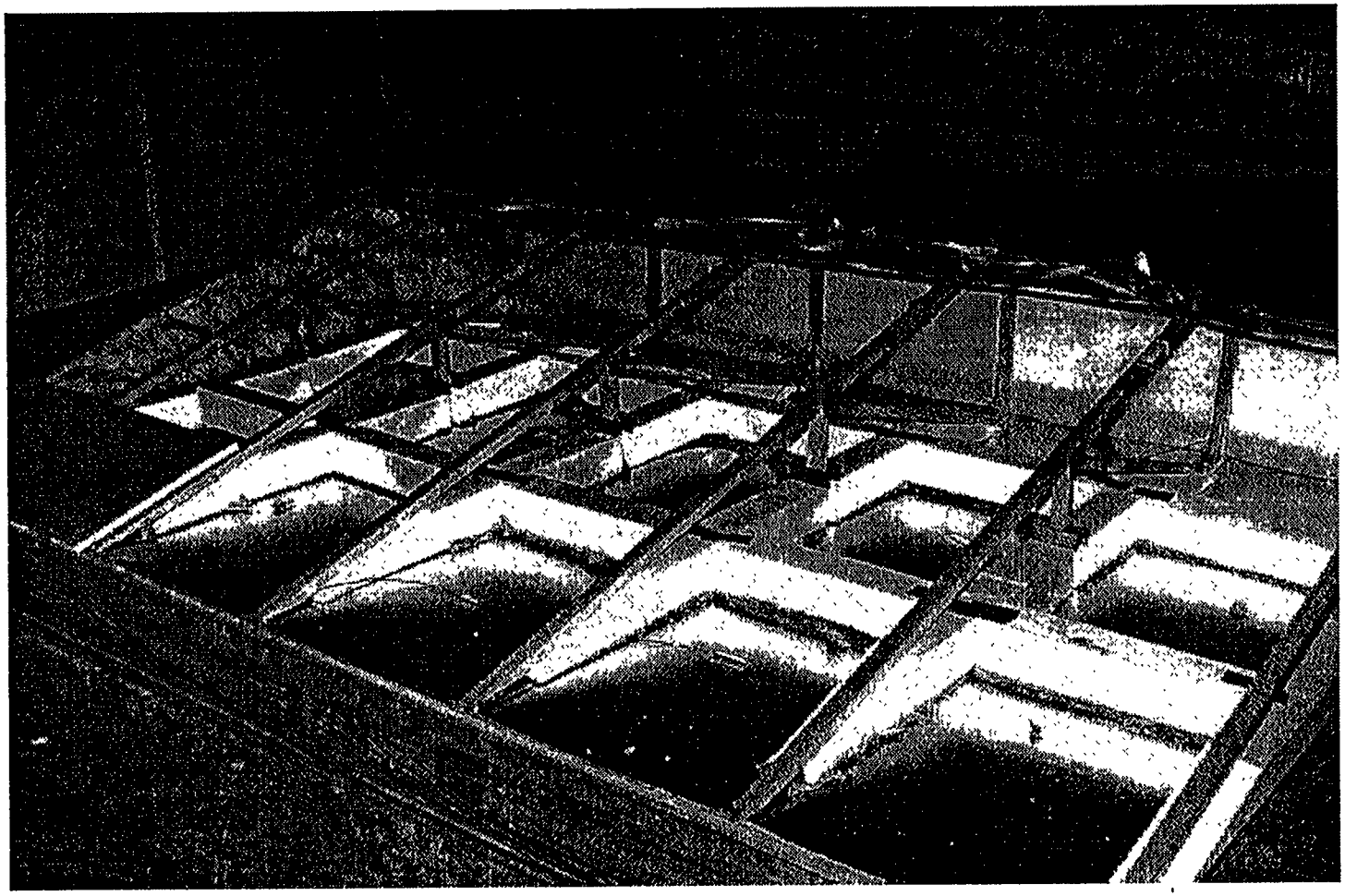

Fig. 11. Photograph of the manufactured home test section, with PEPs installed, after attempts to improve insulation coverage.

Figure 12 shows the results from this series of tests with the four layers of fiberglass added to the data in Fig. 10 from the first two series of tests. The range of insulation mean temperatures has been extended slightly from the range in Fig. 10 to include data for Run S2Cr. Only center-of-cavity data were obtained in the original S2C and they agreed to three significant figures with the data for S2Cr. The data drawn as open circles for the four nominal R_{US}-7 fiberglass batts show that the rumble blanket is not quite as effective in the center of the cavity as another layer of insulation on top of the ceiling. If four layers of this insulation were expanded and working in series like two layers, the R-value for four layers would be twice that for two layers. Data in Fig. 12 show four layers to be 1.85 to 1.95 times as good as two layers, despite the effect of R-value from the dead air in the gaps between the third layer and the rumble blanket. A possible explanation is that the rumble blanket is not expanded between the trusses as much as the layers on the ceiling because the roof holds the rumble blanket in place over the trusses. With the roof in place, it was impossible to visually inspect the rumble blanket.

Considering the whole system, the rumble blanket works as a thermal break in the bridge through the trusses, especially near the eave edge. The system R-values for the four fiberglass batts are a significant improvement over what was achieved for two layers alone and for the PEPs atop one layer: system R-values at winter conditions from R_{US}-16.8 to 18.6 (R_{SI}-3.0 to 3.3) and 15.9 (2.8) at the summer condition rather than between 12.0 and 12.7 (2.1 and 2.2). The ratios to the higher center-of-cavity R-values are 55 to 59% both winter and summer. The radiant barrier effect with two layers of batts was not noticed with the rumble blanket against the roof. Moreover, the addition of the 0.75-in. (1.9-cm) thick XPS sheathing (with nominal R_{US}-3) just to the vertical eave edge in Run W2Cx produced an extra R_{US}-1.6 (R_{SI}-0.28) for the system and improved the system R-value by 9% to R_{US}-19.2 (R_{SI}-3.4) This point is shown as a solid circle in Fig. 12.

4.3. OVERALL COMPARISONS FOR CONFIGURATIONS A, B AND C

The results of an additional calculation of system R-value are shown as a solid star on Fig. 12. HUD manufactured housing construction and safety standards require compliance with an upper limit on the overall U value of the roof/ceiling, walls and floor. The limit varies with location, specified as one of four zones in the continental United States. For the roof/ceiling, center-of-cavity insulation R-values and inside and outside film resistances, all at 75°F (24°C), are used with parallel path corrections for insulation compression and framing effects. The method is specified in a companion HUD manual (Conner 1992). For this test section, including the stub wall on the eave edge, the system R-value for insulation Configuration A by this method, called the HUD method in Fig. 12, is estimated to be R_{US}-14.8 (R_{SI}-2.6). This is 21% higher than the measured temperature-independent average of 12.2 for this system. In fact, by rough interpolation of the system results for Configurations A and C, a fiberglass batt system comprising two layers on the ceiling and a rumble blanket would be required to match results by the HUD method for two layers alone on the ceiling.

The temperature variation of the center-of-cavity R-values for Configurations A and C are consistent with each other and with the expected decrease in the thermal resistivity of fiberglass as temperature increases. Lack of variation with mean insulation temperature of the system R-values at

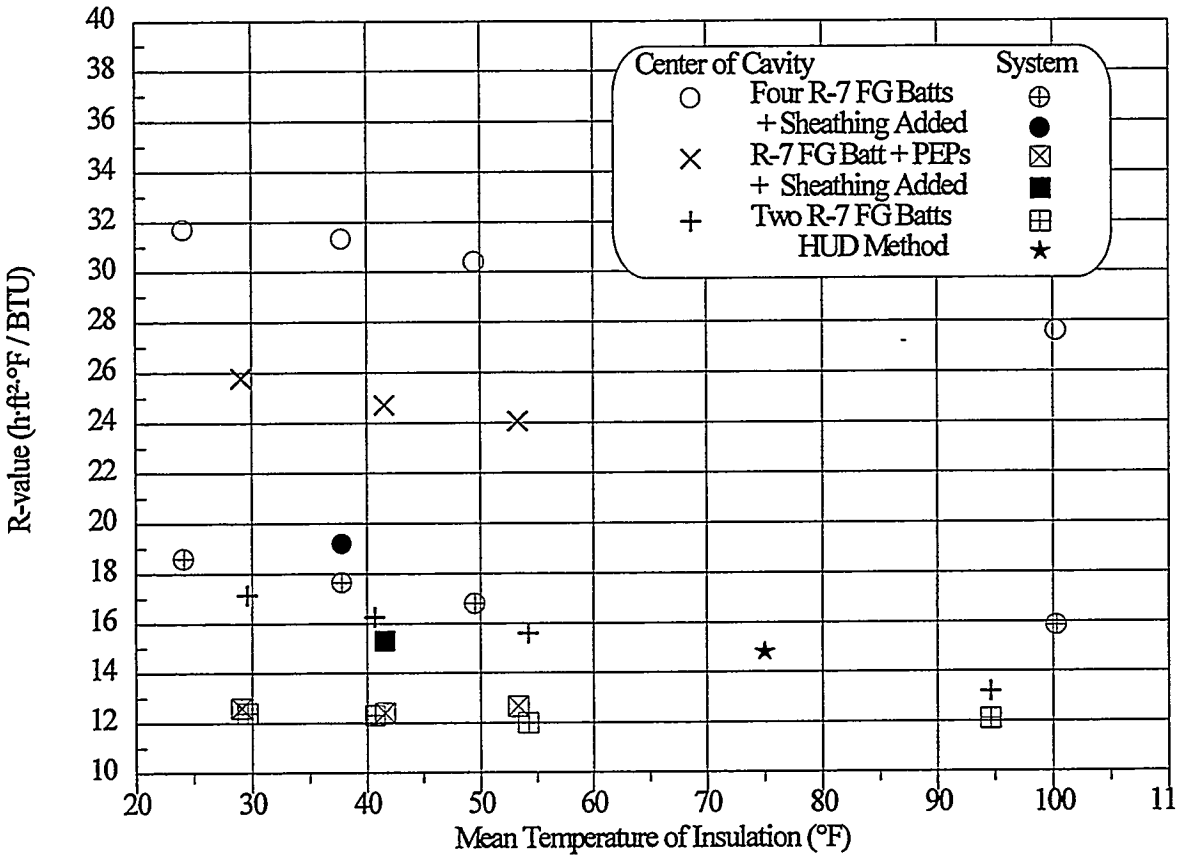

Fig. 12. Comparison of the R-value across each of the three fiberglass batt-based insulation configurations with its system R-value.

winter conditions for Configurations A and B indicates that the non-temperature dependent effects at the edge and through joists and joints dominate.

Although the system with PEPs shows the lowest ratio of system to center-of-cavity insulation R-value of the three fiberglass-based configurations, it provides high insulation value in the vertical direction near the eave edge. To illustrate this feature, Fig. 13 compares data for R-values across the insulation above HFT 1, at the edge of the nominal 2 × 4 top plate, with R-values across the uncompressed insulation in the center of cavity. The shaded lower bars show apparent R-values at the edge, produced from the measured temperature differences across the insulation at the edge divided by the heat flux from HFT1. The unshaded bars show the center-of-cavity R-values from Fig. 12. The trend for the center-of-cavity R-values going from Configuration A to B to C is clearly different from the trend through HFT 1 at the edge. HFT1 was not at the edge of the top plate for tests W1A and W3A. To get the data shown as dashed lines, data for all three conditions with Configuration C were used to establish a slope vs. condition and, with data for W2A, produced the estimated data for W1A and W3A. The shaded and bolded bars for Configuration B at the edge show higher R-values than do the shaded bars for either Configuration A or C. The claim, based on the photograph in Fig. 1, is that Configuration B with the PEPs causes no significant compression effects at the edge. The two layers in Configuration A are moderately

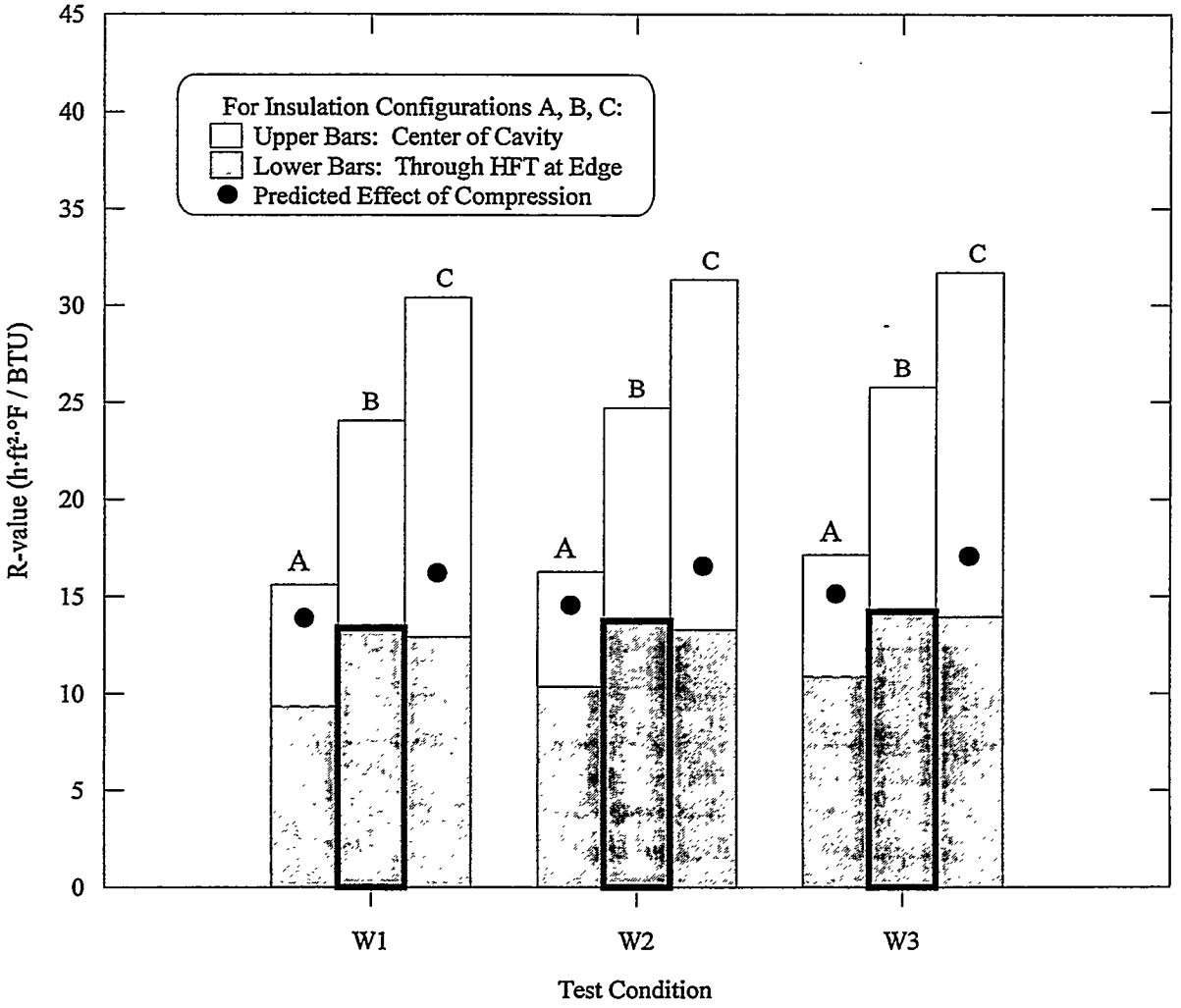

Fig. 13. Effect of insulation compression at the eave edge on the apparent R-value for Configurations A and C compared to the lack of effect for Configuration B.

compressed at the edge. There is severe compression for Configuration C. However, all configurations show the effect of the horizontal thermal bridge at the edge, which keeps the gypsum under HFT 1 cooler than under HFTs 2 or 3 and indicates more heat flux through HFT1. For Configurations A and B, the predicted effect of compression is shown by solid circles at each condition. These R-values are calculated from the thickness divided by thermal conductivity from Eq. (1) as a function of temperature and density. The remaining amount of difference from the solid circle to the top of the shaded bar is due to horizontal effects at the edge. Configuration A, which does not do as good a job of insulating the edge as Configuration C, shows that more of the difference must be explained by horizontal effects. All of the difference for Configuration B must be explained by horizontal effects. For this configuration, the eave edge is not filled with insulation. It is reasonable that Configuration B shows the most decrease in R-value that must be explained by a horizontal thermal bridge at the edge.

4.4. TESTS WITH BLOWN-IN ROCK WOOL (CONFIGURATION D)

Subsequent to the initiation of tests with the fiberglass batt configurations in the manufactured home test section, our industrial CRADA partner began to insulate attics with blown-in rock wool. We added a test series with this same product to compare to the fiberglass batt-based series. Of particular interest was the ability of blown-in insulation to cover the ceiling joists uniformly except where the slanted and vertical truss members connected to the joists. Insulation was added to the rock wool in this series, including EPS boards and PEPs, but it was placed over the top of the trusses instead of on top of the rock wool.

It was more difficult to duplicate the rock wool configuration used by our industrial partner than it was to duplicate their two layer fiberglass batt configuration. Several bags of the rock wool they use were obtained from them and we observed their technique of installing it. We had them fill a box of known volume and determined that their average as-blown density was 2.5 lb/ft^3 (40 kg/m^3). We have the same make of blowing machine as they and used the same settings for air pressure, gate opening and auger speed. Our technique yielded 2.4 lb/ft^3 (38 kg/m^3) as the average density in our small test section, with a value of 2.3 lb/ft^3 (37 kg/m^3) measured in the center of cavity. The information on the label for each bag of the product implies that the as-blown density should be 1.4 lb/ft^3 (22 kg/m^3). We attempted unsuccessfully by blowing machine adjustments and by passing material through the machine twice to achieve this low density. Since our industrial CRADA partner achieved about the same density as we did, the average density of 2.4 lb/ft^3 (22 kg/m^3) was accepted.

Our industrial CRADA partner puts in enough material per unit area of attic, with no allowance for truss volume, to achieve an average R-value of R_{US}-21 h·ft^2·°F/BTU (R_{SI}-3.6 m^2·K/W) at a density of 1.4 lb/ft^3 (22 kg/m^3) and temperature of 75°F (24°C). We installed the same amount per unit area, also with no allowance for truss volume, and achieved an average thickness of 4.1 in. (10.4 cm) with a center of cavity thickness of 4.6 in. (11.7 cm). There was less thickness near both the eave and the ridge. Excess rock wool blown over the trusses near the eave was pushed toward the middle of the test section to avoid compression when the roof was put back. The average thickness in the 20% of the test section near the eave was measured as 3.4 in. (8.6 cm). Our blowing technique for this small test section yielded greater insulation thickness in the middle of the test section than near the ridge. After pushing material higher than the trusses near the edge back toward the middle, the middle and ridge coverage was evened out manually. Measurements at the end of the tests showed an average thickness for the 40% of the test section near the ridge of 3.8 in. (9.7 cm).

Our center-of-cavity R-value, interpolated to 75°F (24°C) from measurements described below, was 12.5 h·ft^2·°F/BTU (2.2 m^2·K/W) . To estimate the center-of-cavity R-value achieved by our industrial CRADA partner, consider Fig. 14. The curve shown as a solid line on the figure is quoted by McElroy *et al.* (1987) as the average from 10 different rock wool products studied by Bomberg. The curve shown as a dashed line is the solid curve less 0.8 at each point in order to pass through our center-of-cavity result and two additional data by Yarbrough and Toor (1983). By ratios to our results and our measurement of our CRADA partner's average density, we estimate their center-of-cavity density as 2.4 lb/ft^3 (38 kg/m^3) and center-of-cavity thickness as 4.4 in. (11.2 cm). Using the dashed curve on Fig. 14, their center-of-cavity R-value is then 12 h·ft^2·°F/BTU (2.1 m^2·K/W). This is less than the nominal R_{US}-14 center-of-cavity

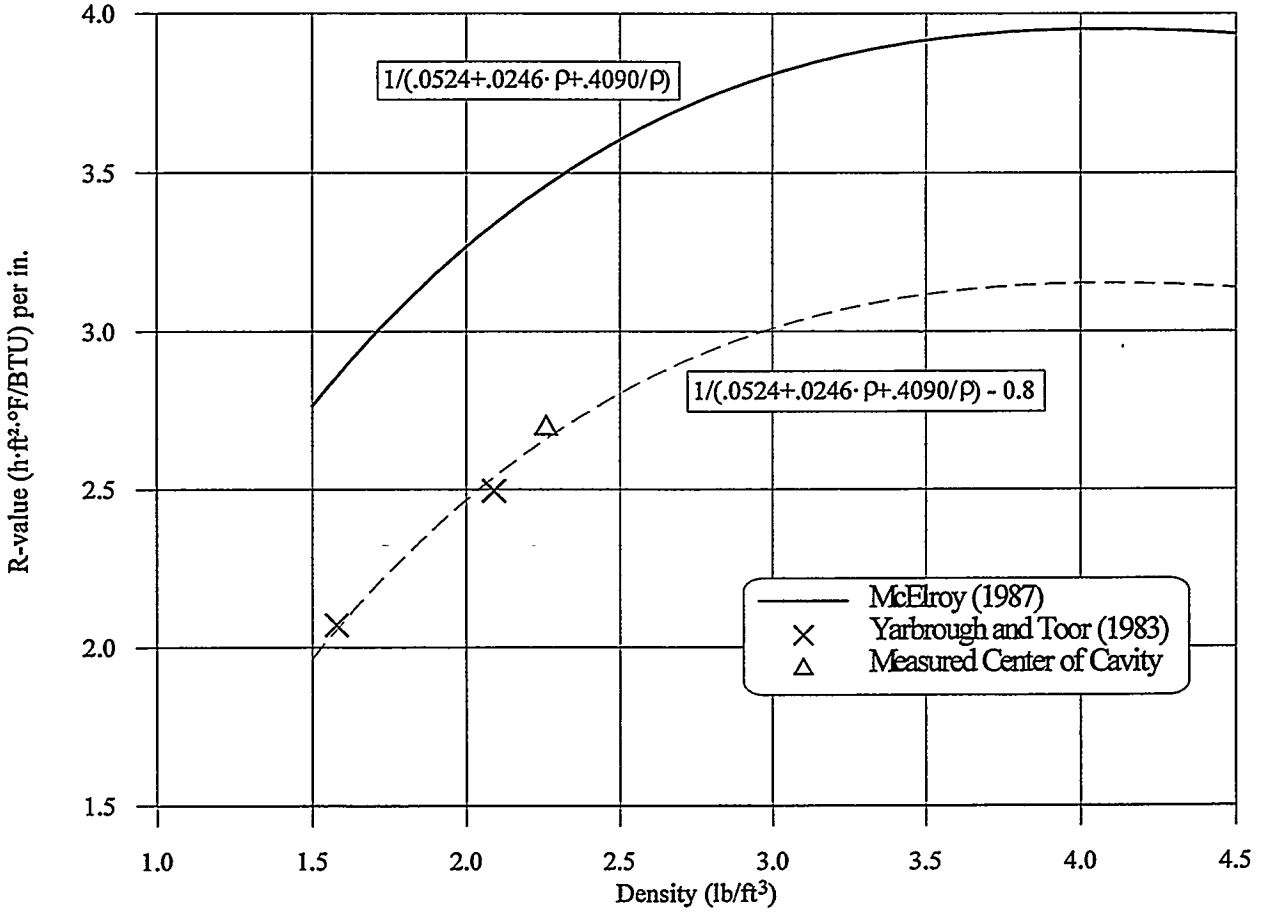

Fig. 14. Effect of density on the R-value per unit thickness of rock wool insulation.

R-value of the two layers of fiberglass batt insulation. More significantly, neither of us is achieving R_{US}-21 that the bag label promises if the as-blown density is 1.4 lb/ft^3 (22 kg/m^3).

Despite the high as-blown density, the rock wool covered the nominal 2 in. × 2 in. (actual 1.5 in. × 1.5 in. or 3.8 cm × 3.8 cm) ceiling joists without gaps except where vertical and slanted truss members were joined to the joists. A series of tests was done with the rock wool under the standard metal roof of the test section to determine system performance, including a check if the ratio of system to center-of-cavity R-value was improved over the 72 to 77% range at winter conditions and 92% at the summer condition with Configuration A. The order of the tests was W2D, W3D, W1D and S2D. System R-values are shown on Fig. 15 along with one of three sets of center-of-cavity results. Two more sets are shown on Fig. 16. The solid curve is a linear regression of the inverse of all the center-of-cavity R-values with mean insulation temperature. At 75°F (24°C) this curve yields the R_{US}-12.2 (R_{SI}-2.1) quoted above. Comparing system results in Fig. 15 to those for the two layer fiberglass batt configuration in Fig. 10, the rock wool system at winter conditions shows more scatter about the average value of R_{US}-9.5 (R_{SI}-1.7). The 95% confidence interval of ±0.5 h·ft²·°F/BTU (±0.09 m²·K/W) estimated for the system R-values of Configurations A and B is the same for Configuration D. Tests W3D and W1D at the low and high winter

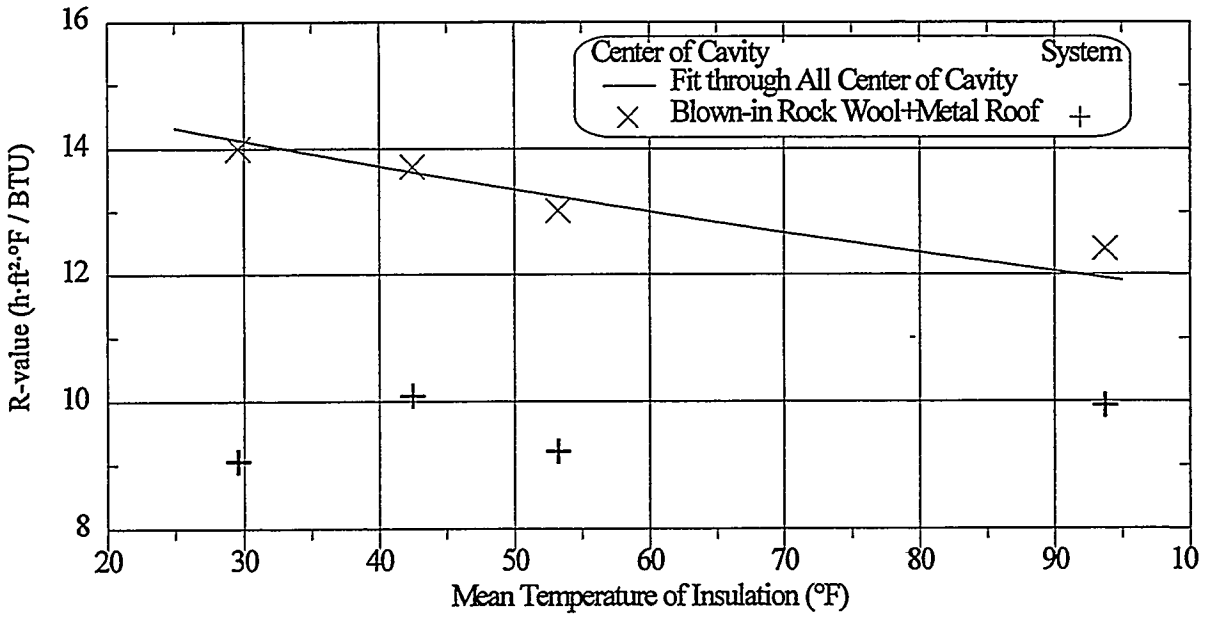

Fig. 15. Comparison of the R-value across the center-of-cavity insulation with the system R-value for Configuration D.

mean temperatures, respectively, show a system R-value at the lower limit of the confidence interval about the average while Test W2D at the middle winter mean temperature shows a system R-value at the higher limit.

A summary comparison of results from the two base-case configurations is as follows:

Configuration		Condition	Center-of-Cavity R_{US} (R_{SI})	System R_{US} (R_{SI})	System/Center (%)
A.	Two FG	Winter	15.6-17.2 (2.7-3.0)	12.0-12.4 (2.1-2.2)	72-77
	Batts	Summer	13.2 (2.3)	12.1 (2.1)	92
D.	Rock	Winter	13.0-14.0 (2.3-2.5)	9.1-10.1 (1.6-1.8)	65-74
	Wool	Summer	12.4 (2.2)	9.9 (1.8)	80

The system/center ratios for the rock wool are lower than for the fiberglass, implying that the average insulation coverage is poorer with the rock wool. Although the rock wool covered the joists more uniformly than the fiberglass batts, our measurements of the smaller rock wool thickness in the 40% of the test section near the ridge showed that it had 17% less insulation than the middle 40% of the test section. Also, the eave edge could be thermally less protected by the rock wool than the fiberglass batts. Because excess rock wool blown over the trusses near the edge was pushed toward the middle of the test section before the roof was rolled back in place, compression of rock wool was avoided but there was 26% less insulation thickness in the 20% of the test section near the eave edge than in the middle 40%. How much effect the edge has on the system/center ratio is discussed later after a model of the edge is constructed and validated.

4.5. TESTS WITH EPS AND PEPS OVER THE TRUSSES AND BLOWN-IN ROCK WOOL IN THE ATTIC CAVITY

The principal lesson from the series of tests of Configuration B, PEPs on top of a layer of fiberglass batts, was that significant framing effects were present with the type of PEPs used in these tests. They left the joists and joints between panels underinsulated. As a prelude to tests with a more continuous layer of PEPs on top of the trusses, a first series of extensions of the base-case runs with Configuration D was done in the order S2Dx1, W2Dx1, W3Dx1 and W1Dx1. Two 0.625 in. (1.6 cm) thick EPS boards were put over the trusses. Joints were sealed with masking tape. The thermocouples from the top of the metal roof were placed on the top layer of EPS. The metal roof was not used. The density of the EPS was measured as 1.09 lb/ft^3 (17 kg/m^3) and the nominal R-value of each layer estimated as 2.3 h·ft^2·°F/BTU (0.39 m^2·K/W) (ASTM 1992). In addition, with about R_{US}-5 (R_{SI}-0.9) of insulation R-value on top of the trusses, the metering chamber energy balance was corrected for flanking losses around the attic space. These losses were estimated from temperature differences and R-values across the guard insulation and included in the corrections before calculating the system R-value by Eq. (2). The attic space was unvented so it should act like a dead air space between the insulation on the ceiling and the insulation over the trusses.

Figure 16 shows the R-values measured with the two layers of EPS over the trusses but no metal roof. The center-of-cavity results shown as bold ×'s are for the rock wool insulation on top of the ceiling during these tests. The best fit line and first set from Fig. 15 are repeated for comparison. The system R-values from Fig. 15 are repeated, too. The system R-values with the additional EPS insulation over the trusses, represented by the bold +'s, show a 9% improvement at winter conditions and a 7% improvement at the summer condition. This is despite the addition of about R_{US}-5 (R_{SI}-0.9) of insulation, that is, almost a 40% increase in the insulation R-value through the center of cavity.

The effect of no metal roof in the first extended runs was investigated in a second series of extended runs S2Dx2, W2Dx2, W3Dx2 and W1Dx2. A layer of wide aluminum foil, marketed as radiant barrier material, was attached with contact cement to the bottom of the lower pieces of EPS. Another layer was laid over the top pieces. Total emittance data for metals yields a reflectance of 95% for polished aluminum while bright galvanized metal has a 77% reflectance (Sparrow 1970). The results for the second extension runs are shown with boxed symbols on Fig. 16. The center-of-cavity results are slightly higher than the values from the first extension runs. The system values are 22% better at the winter conditions than the base-case values and 29% better at the summer condition.

For the extended runs with the blown-in rock wool, some thermocouples were moved from the top of the roof to locations under the bottom layer of EPS then under the bottom foil. Others were moved to the middle of the EPS. Some of these relocated thermocouples allowed temperature differences ΔT to be measured across the attic air space when EPS layers then foil were added. Assuming that the heat flux q through the center of cavity away from the eave edge flows up through the roof, effective R-values for the air space were estimated by $\Delta T/q$ for the situations with the metal roof, with no metal roof and with the foil under and over the EPS layers. The resulting effective R-values of this unvented attic air space are as follow:

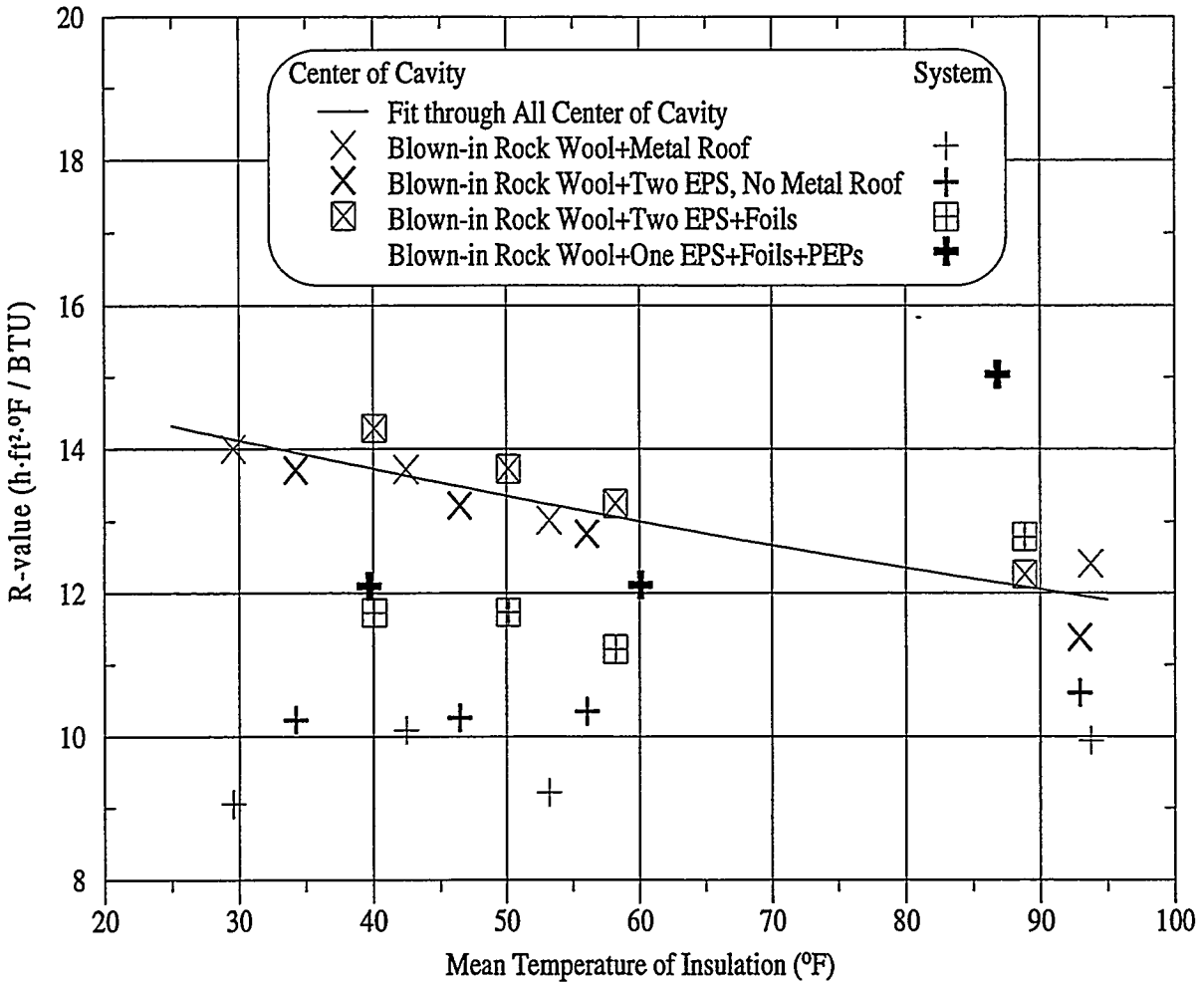

Fig. 16. Results for runs with Configuration D including addition of EPS, foils and PEPs on top of the trusses.

Roof Configuration	Winter R_{US} (R_{SI})	Summer R_{US} (R_{SI})
Base Case: Metal Roof Only	3.3 (0.6)	5.9 (1.0)
Extension 1: Two EPS Layers	1.3 (0.2)	1.3 (0.2)
Extension 2: Two EPS + Foils	2.3 (0.4)	7.3 (1.3)

It appears that any potential increase in the system R-value in the first extension runs due to the addition of about R_{US}-5 (R_{SI}-0.9) by the EPS layers is effectively negated by the lack of a radiant barrier effect with no metal roof, especially for the summer condition. The presence of the bottom foil noticeably helps the winter air space effective R-value and significantly helps the summer one. Yet, in both extension runs, the system R-value does not benefit by R_{US}-5 (R_{SI}-0.9) because the underprotected eave edge presents a lower resistance path for heat flow between the climate and metering chambers that becomes more preferable as the effective attic space and roof insulation R-values increase.

A final set of runs with the rock wool insulation was done with the top layer of EPS on the trusses replaced by a layer of PEPs, which was covered by the top foil. The PEPs were placed alternately foil side up and down in a checkerboard pattern. This placement allowed sufficient overlap of the PEPs so there should have been little effect of the thin foil strips at the edges on the R-value through the PEPs. Recall from Fig. 9 that the center-of-cavity R-value for the PEPs used in this study was about 16 $h \cdot ft^2 \cdot °F/BTU$ (2.8 $m^2 \cdot K/W$). Unfortunately, the PEPs were slightly warped after the tests with Configuration B so placing them alternately with foil side up and down still caused air gaps between PEPs. Compared to the base-case results, the improvement in system R-values with the PEPs was 20% for the winter conditions and 51% at the summer condition. Figure 16 includes these data, shown as very bold +'s.

The lesson from simple parallel path methods and reinforced by these measurements is that it is futile to try to improve system R-value by adding center-of-cavity R-value when significant thermal bridges or reductions in insulation R-value exist. In these extensions to the base-case tests with the blown-in rock wool insulation, the eave edge remained thermally underprotected. With the PEPs inside the attic space, a somewhat practical fix was to add sheathing at the edge and over the joints between PEPs. Figure 12 showed that this improved the system R-value by 23% at winter conditions. With the whole top of the test section insulated by a layer of EPS and PEPs, a more drastic and less practical fix was tried to match the amount of edge insulation to that over the trusses. Additional boards of EPS like the ones shown in Fig. 2, which insulated the ridge edge and the lower part of the stub wall at the eave edge, were stacked at the eave edge so they protected all of it like the ridge edge. The boards were almost as wide as the board guarding the lower part of the edge and extended several inches above the top of the roof at the edge. There was a gap between the edge and the top board because the PEPs extended slightly over the eave edge. Nonetheless, at the mid-winter condition, the system R-value for this final situation was R_{US}-14.3 (R_{SI}-2.5); at the summer condition, it was R_{US}-19.4 (R_{SI}-3.4). These R-values are 51% and 95% better, respectively, than the base-case results with only the metal roof over the trusses and rock wool insulation over the ceiling.

5. MODELING WITH HEATING 7.2 AND ASEAM 3.0

5.1. EDGE MODEL

The experiments have shown that better insulating features at the eave edge could be important for improving the thermal performance of the roof/ceiling in a manufactured home. To evaluate the efficacy of such features, valuable insight can be gained by knowing the heat flow through the edge. Unfortunately, local measurements with an HFT at the edge did not yield reliable data because of the two- and three-dimensional effects that seemed to occur there. The total measurement for the test section did not give the detail necessary to isolate the effects at the eave edge from effects over the joists and, for the PEPs, over the joints in the insulation.

HEATING 7.2 (Childs 1993), a three-dimensional, transient heat conduction program, was used to model the 24 in. (0.61 m) width between the centers of two adjacent joists for insulation Configurations A and B. Horizontally, the model of the edge included the region from outside the test section to a vertical plane 4.125 in. (10.5 cm) toward the ridge edge measured from the inside corner of the ceiling. Vertically, the region extended from just above the roof to a horizontal plane down 7.5 in. (19.1 cm) from the inside of the ceiling. The components of the test section in this region included all of the insulation compressed by the roof in Configuration A and enough of the stub wall to include all the heat flowing through it. The thermal properties of the construction materials and insulations are considered well known from values in the literature (ASHRAE 1993) or from our measurements. Thus, the accuracy of the edge model is primarily dependent on how well the complicated geometry is modeled and how well the boundary conditions are specified. The latter is a particularly difficult task because of the geometry itself, which causes uncertain flow patterns over the boundary surfaces as air circulates in the climate and the metering chambers.

To validate the model, our approach was to model the edge region, impose the measured inside and outside air temperatures and run the model on test cases. Several temperatures were measured for use in the validation process. As detailed above in Fig. 6 and the description of instrumentation in the test section, there were five thermocouples near and on the corner of the ceiling at the eave edge. Thermocouples were located outside the test section on the aluminum siding at the level of and below the top plate. There were also thermocouples inside the attic space at the edge where the perimeter rail and the top of the gypsum ceiling met.

Four test cases were run. Climate chamber and metering chamber temperatures were those of Condition W2, specifically, air temperatures of 1.6°F (-17°C) outside and 75°F (24°C) inside the test section for tests with Configurations A and B. Figure 17 shows sketches of the features of the edge in the model of the two-layer fiberglass configuration for Test W2A, the configuration for Test W2B with PEPs before extra sheathing was installed, and both parts of the extended Run W2Bx with sheathing over the joists and joints between PEPs. One part had XPS sheathing, too, both vertically and over the trusses at the edge (W2Bxb). The other part had only the vertical sheathing in addition to the joist and joint sheathing (W2Bxv). The horizontal and vertical arrows on the sketches mark two of the three axes of the coordinate system used in the model. The third axis extended 24 in. (0.61 m) into the plane of the

Two R-7 FG Batts (Test W2A)

Condition W2;
no sheaths

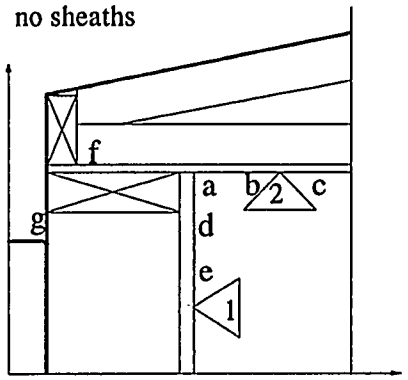

T(°F)	Meas.	Model
a	62.9	66.2
b	67.8	71.6
c	69.8	72.4
d	65.1	69.1
e	68.9	71.7
f	25.4	26.3
g	13.0	17.5
Q_1 = 32.9 BTU/h		
Q_2 = 16.0 BTU/h		
Q_{total} = 314±23 BTU/h		

R-7 FG Batts + PEPs (Test W2B)

Condition W2;
no sheaths

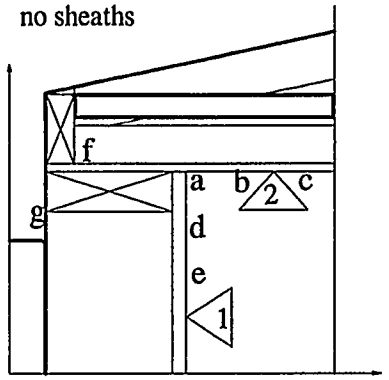

T(°F)	Meas.	Model
a	63.6	66.2
b	68.4	72.1
c	70.4	73.0
d	65.3	68.9
e	68.9	71.6
f	25.3	22.7
g	12.6	15.6
Q_1 = 34.0 BTU/h		
Q_2 = 15.3 BTU/h		
Q_{total} = 311±22 BTU/h		

R-7 FG Batts + PEPs (Test W2Bxb)

Condition W2;
both vertical and truss
sheaths

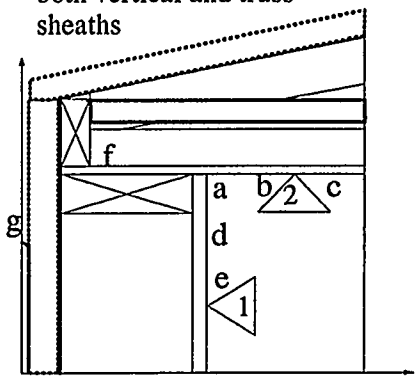

T(°F)	Meas.	Model
a	66.4	67.4
b	69.9	71.6
c	71.5	73.0
d	67.8	69.8
e	70.8	72.2
f	35.3	32.1
g	11.5	13.6
Q_1 = 28.2 BTU/h		
Q_2 = 13.1 BTU/h		
Q_{total} = 252±19 BTU/h		

R-7 FG Batts+ PEPs (Test W2Bxv)

Condition W2;
vertical sheath only

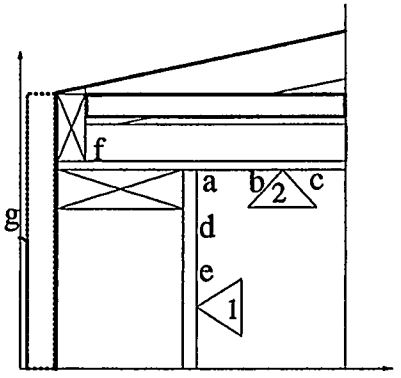

T(°F)	Meas.	Model
a	66.0	67.6
b	69.7	72.3
c	71.3	73.1
d	67.4	70.0
e	70.6	72.2
f	33.4	33.3
g	11.1	14.3
Q_1 = 28.3 BTU/h		
Q_2 = 14.4 BTU/h		
Q_{total} = 260±17 BTU/h		

Fig. 17. Temperatures from the edge model of the manufactured home test section compared to measurements.

sketches. The origin of the horizontal axis was chosen to leave room to the right of the origin for the vertical XPS sheathing that was present in two cases. Locations on the model where temperatures were measured are labeled with letters 'a' through 'g'. The temperatures for locations 'a' through 'e' inside the ceiling space were from single thermocouples. Temperatures for 'f' are the average from two thermocouples while those for 'g' are from eight thermocouples. Combinations of reasonable convective boundary conditions, specifically, values of the film heat transfer coefficient on the model of the inside ceiling and wall surfaces, the outside vertical edge, and the slanted roof edge, were tried until the best agreement between measured and predicted temperatures was obtained. What is meant by the best agreement is described below.

The program generated the total heat flow through a 7.5 × 24 in. (19 × 61 cm) portion of the inside of the stub wall, designated by a '1' inside a triangle, and through a 4.125 × 24 in. (10.5 x 61 cm) portion of the ceiling, designated by a '2' inside a triangle. For convenience in interpreting these data compared with Q_{total}, the total heat flow from the experiments, they were multiplied by four to include all 8 ft of the edge and entered as Q_1 and Q_2, respectively, in the data tables next to each sketch. The values for Q_{total} have been corrected for heat exchange between the guard and metering chambers and heat flows through the insulated surfaces around the perimeter. They are averages of data recorded at four-minute intervals over the steady-state portion of each test. At least 12 hours of steady-state data made up each average. Like the estimate for the system R-value, the 95% confidence interval given for each value is estimated as twice its standard deviation over this time.

Before discussing the implications of the data in Fig. 17, a brief explanation is in order to give the rationale for choosing the model. Small rectangular regions containing appropriate materials were built up to model the construction. Properties for the materials were specified at the appropriate average temperature for the tests at Condition W2 (about 40°F or 4.4°C). Convective heat transfer coefficients were specified and varied to include the range from free convection to moderate forced convection. The results shown in Fig. 17 correspond to free convection both inside and outside the test section. On the inside, the heat transfer coefficient was 1.5 BTU/(h·ft²·°F) [8.5 W/(m²·K)]; on the outside, the value on the vertical surface was 0.5 BTU/(h·ft²·°F) [2.8 W/(m²·K)] and the value was 0.25 BTU/(h·ft²·°F) [1.4 W/(m²·K)] on the horizontal surfaces of the steps that modeled the slanted roof. The vertical surfaces were assumed to be adiabatic. These are judged the best set of values because raising the heat transfer coefficients on the outside (in the climate chamber with high velocity circulation fans) by 100% lowered the temperatures calculated at locations 'a' through 'e' but they remained above the measured temperatures, while the outside temperature 'g' dropped below the measured value. Then, lowering the heat transfer coefficients on the inside (in the metering chamber with low velocity circulation fans) by 33% lowered the inside temperatures so that they were about 0.5°F (0.3°C) closer to the measured temperatures than the best values gave. However, the outside temperatures were 2 to 4°F (1 to 2°C) below the measured averages there.

Figure 18 shows the agreement that was achieved between measured and calculated temperatures at locations 'a' through 'e' and at 'g'. The calculated temperatures are all above the measured values, but by about the same amount both inside and outside in each case. Thus, the model should have the same surface to surface temperature differences as the tests. Predicted heat flows for the edge are therefore assumed to be as accurate as the total measured heat flows. Moreover, for the chosen combination of heat

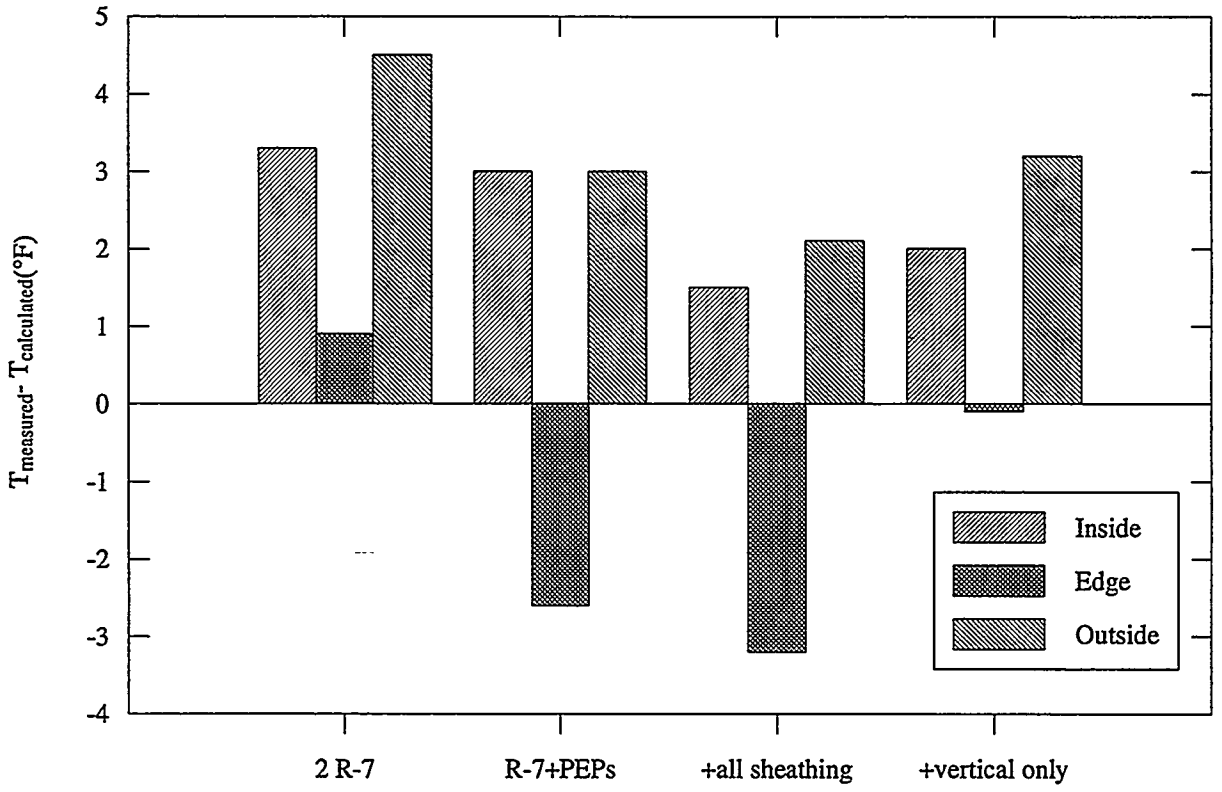

Fig. 18. Relationship between the measured and predicted temperatures to validate a model of the eave edge of the manufactured home test section.

transfer coefficients, the edge temperature 'f' from the model is above the measured one for Test W2A (2 R-7), below it for W2B (R-7+PEPs) and W2Bxb (+ sheathing vertically and over the trusses at the edge), and equal to it for W2Bxv (+vertical sheathing only). The trials with other combinations of heat transfer coefficients yielded predicted edge temperatures that were below the measured values in all cases.

With the detailed heat flow through the inside surfaces of the edge of the test section available from the model, several observations can be made. The heat flow through the inside wall labeled as Surface 1 is 10.9% (within ± 0.4%) of the total flow for all four cases. The heat flow through the portion of the ceiling labeled as Surface 2 is 5.2% (within ± 0.3%) of the total flow for all four cases. Thus, 16% of the total heat flow in all the test cases is due to the edge. For Tests W2A and W2B without vertical sheathing, the heat flows through the inside walls, Q_1, are the same to well within ±2 to 3 BTU/h, which is 6 to 8% of Q_1. The 95% confidence intervals in Q_{total} expressed as a percentage of Q_{total} are 6 to 8%. For Tests W2Bxb and W2Bxv with vertical sheathing, the Q_1 values are the same. The heat flows through the ceiling, Q_2, vary as expected, from the largest value for W2A with two compressed layers of fiberglass batts to the smallest value for W2Bxb with PEPs on top of a layer of fiberglass batts and XPS sheathing both vertically and on top of the slanted roof trusses at the edge. The ceiling heat flows for cases W2B and W2Bxv fall between these extremes in the correct order. The influence of the vertical sheathing in W2Bxv makes the heat flow through the ceiling slightly smaller than in W2B with no sheathing.

To gain additional insight to the detailed behavior of the heat flow through the eave edge of the test section and further validate the model, Fig. 19 compares measurements and predictions in tests without sheathing at the extremes of the winter conditions that were imposed. For Tests W1A and W1B, air temperatures were 26°F (-3°C) outside the test section and 75°F (24°C) inside. For Tests W3A and W3B, air temperatures were -25°F (-32°C) outside and 75°F (24°C) inside. Not all of the temperatures on Surfaces 1 and 2 were measured in Test W3A. For Test W1A, the ratios of predicted heat flows on Surfaces 1 and 2 to total heat flow are lower than the ranges in Fig. 17. The measured heat flow for this case is high compared to the total heat flow for W1B. The difference is +20 BTU/h. At Condition W2 in Fig. 17, the difference between total heat flows for W2A and W2B is +3 BTU/h. In Fig. 19, the difference between W3A and W3B is +5 BTU/h. The difference for Condition W1 is still within the uncertainty of Q_{total} for W1A but large relative to the differences for Conditions W2 and W3. Otherwise, the comparisons between measured and predicted temperatures and measured total heat flow and predicted heat flows for Surfaces 1 and 2 are as they were in Fig. 17. The accuracy of the simulation seems unaffected by the temperature dependence of thermal properties. The same insulation properties were used in Figs. 17 and 19; in particular, thermal conductivities of fiberglass were inserted at a temperature of about 40°F (4°C).

The model was used to predict edge heat flows for Tests W1D, W2D and W3D with blown-in rock wool. The geometry was the same as for Configuration A except uncompressed rock wool occupied the volume between the ceiling joists or gypsum ceiling and the roof or trusses near the eave edge. The thermal conductivity of rock wool was inserted at 40°F (4°C) from the inverse of the R-value per unit thickness measured in the tests with Configuration D. As Table 2 shows, the rock wool allowed slightly more heat to flow through the edge than the two layers of fiberglass batts for comparable conditions, but the total heat flows measured with the rock wool were significantly larger than with the fiberglass. Therefore, the heat flows through the edge were a smaller fraction, 13.2 ± 0.9%, of the totals for the rock wool.

To present the results for the edge heat flows in terms of a framing effect for the flat ceiling only, the sum of the heat flows through Surfaces 1 and 2 in Figs. 17 and 19 and from the runs for rock wool can be subtracted from their respective total heat flows. The result is $Q_{ceiling}$, the heat flow through the ceiling away from the edge. $Q_{ceiling}$ should be free from any edge effects. A framing effect $FE_{ceiling}$ is defined as

$$FE_{ceiling} = 1 - R_{ceiling}/R_{center} \tag{4}$$

where $R_{ceiling} = \Delta T \cdot A_{ceiling}/Q_{ceiling}$ by Eq. (2) and $R_{center} = \Delta T/q_{center}$. The area of ceiling away from the edge is $A_{ceiling} = 48.1$ ft^2 (4.47 m^2) and does not include the area of Surface 2 in the model. The temperature difference ΔT and the heat flux q_{center} are available from the experiments. $FE_{ceiling}$ displays how much the maximum R-value through the clear insulation is reduced by the effect of joists, truss supports, gaps in the insulation between panels and over the joists (in the case of the PEPs) and less insulation near the ridge (for the rock wool).

Two R-7 FG Batts (Test W1A)

Condition W1;
no sheaths

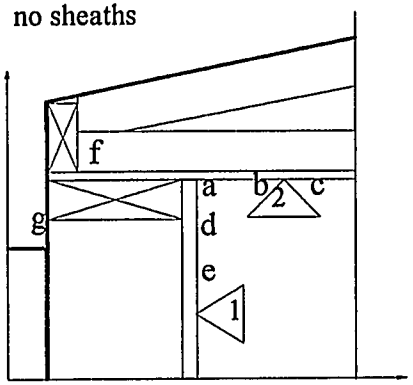

T(°F)	Meas.	Model
a	64.4	69.1
b	70.5	72.7
c	71.4	73.3
d	67.8	71.0
e	71.0	72.8
f	40.5	42.4
g	33.1	36.6
Q_1 = 22.0 BTU/h		
Q_2 = 10.7 BTU/h		
Q_{total} = 223±23 BTU/h		

R-7 FG Batt + PEPs (Test W1B)

Condition W1;
no sheaths

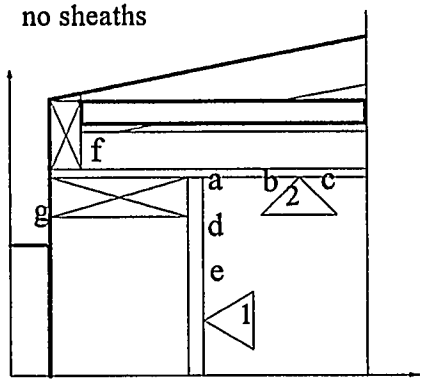

T(°F)	Meas.	Model
a	67.1	69.1
b	70.5	73.1
c	72.0	73.7
d	68.3	70.9
e	71.1	72.7
f	41.0	40.1
g	33.1	35.3
Q_1 = 22.8 BTU/h		
Q_2 = 10.3 BTU/h		
Q_{total} = 203±18 BTU/h		

Two R-7 FG Batts (Test W3A)

Condition W3;
no sheaths

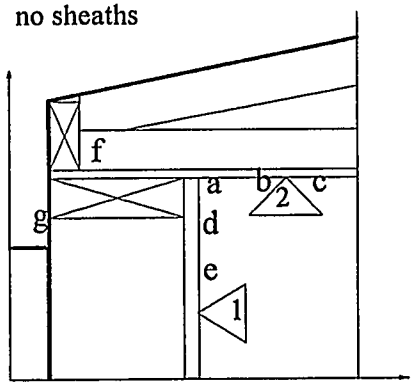

T(°F)	Meas.	Model
a	55.6	63.1
b	n.a.	70.4
c	n.a.	71.4
d	n.a.	66.9
e	66.2	70.5
f	5.8	8.7
g	-9.0	-3.4
Q_1 = 44.8 BTU/h		
Q_2 = 21.8 BTU/h		
Q_{total} = 423±25 BTU/h		

R-7 FG Batts + PEPs (Test W3B)

Condition W3;
no sheaths

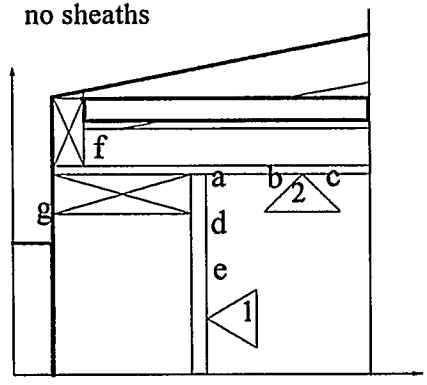

T(°F)	Meas.	Model
a	59.8	62.9
b	66.1	71.1
c	68.8	72.2
d	62.0	66.7
e	66.5	70.3
f	8.2	3.8
g	-9.6	-5.9
Q_1 = 46.3 BTU/h		
Q_2 = 21.0 BTU/h		
Q_{total} = 418±27 BTU/h		

Fig. 19. Application of the edge model of the manufactured home test section to the highest and lowest temperatures imposed for winter conditions.

Table 2. Framing effects for the ceiling of the manufactured home test section.

Test	Q_{edge}(BTU/h) / Q_{total}(BTU/h)	Pred. $R_{ceiling}$ (h·ft²·°F/BTU)	Meas. R_{center} (h·ft²·°F/BTU)	$FE_{ceiling}$
W1A	32.7 / 223	12.4	15.6	0.21
W2A	48.9 / 314	13.3	16.3	0.19
W3A	66.6 / 423	13.5	17.2	0.21
W1B	33.1 / 203	14.2	24.1	0.41
W2B	49.3 / 311	13.5	24.7	0.45
W2Bxb	41.3 / 252	16.7	24.7	0.32
W2Bxv	42.7 / 260	16.2	24.7	0.34
W3B	67.3 / 418	13.7	25.8	0.47
W1D	36.6 / 284	9.7	12.7	0.23
W2D	53.7 / 381	10.8	13.3	0.19
W3D	72.9 / 576	9.5	13.6	0.30

For insulation Configurations A, B and D, Table 2 summarizes the ratios of predicted edge heat flow to measured total heat flow and presents $R_{ceiling}$ for the area of ceiling away from the edge and the corresponding R_{center} from the heat-flux transducers under the center-of-cavity insulation. Equation (4) is used to calculate the framing effect. Configurations A and D show smaller framing effects than Configuration B with the PEPs and their severe joint and joist effects. The framing effects for Configuration D are slightly higher than for Configuration A despite the better insulation coverage near the joists for Configuration D. As discussed earlier, measurements for Configuration D after the tests revealed 17% less insulation thickness near the ridge relative to the center-of-cavity thickness, negating the effect of the better coverage of the joists by Configuration D. The scatter in the values of $FE_{ceiling}$ for Configuration D is a symptom of scatter in system R-values seen already in Fig. 15.

A valuable application of the model of the eave edge of the manufactured home test section is to explore alternate constructions without incurring the time delay and expense involved in direct measurement. In Fig. 20, the results of one such application are shown. The nominal 2 × 4 top plate and the perimeter rail have been removed and replaced by an L-shaped beam. This beam gives horizontal and vertical support to the trusses, which are also shortened by 1 in. (2.5 cm) at the eave edge. The result should be a structure that is as strong as the current one in which the trusses are nailed to the perimeter rail and then the rail and trusses are toenailed to the top plate. This new construction creates space for a special cap made of foam insulation. The cap thermally protects the edge both horizontally and vertically, but does not change the width or height of the roof. Conditions for Tests W2A and W2B were imposed. For additional insulation in the vertical direction and for comparison to the results in Fig. 17, PEPs were specified near the edge as was another layer of fiberglass above them.

2 R-7 FG Batts + PEPs at Edge
Condition W2;
Special Foam Cap and L Beam

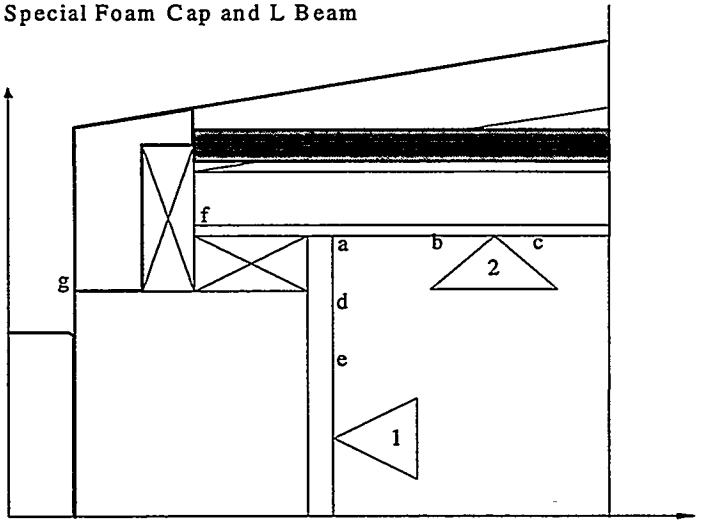

T(°F)	Model
a	67.6
b	72.6
c	73.4
d	69.8
e	71.9
f	35.1
g	15.8
Q_1 = 30.7 BTU/h	
Q_2 = 11.9 BTU/h	

Fig. 20. Application of the model to the eave edge when it is thermally protected by a special cap fabricated from foam insulation.

The predicted inside and outside temperatures in Fig. 20 agree best with the case of a layer of fiberglass under PEPs in Fig. 17. The edge temperature at point 'f' is warmer than any other temperature 'f' in Fig. 17. The heat flow through the inside ceiling (Surface 2) is lower than any other Q_2 in Table 2. Both pieces of evidence point to the good thermal protection that the new edge provides against the flow of heat in the vertical direction. The heat flow through the inside wall (Surface 1) is significantly lower than in the cases with no vertical sheathing but not quite as low as use of the full vertical sheathing permits.

5.2. CEILING JOIST MODEL

HEATING 7.2 was run for a 24 in. (0.61 m) wide section of the ceiling space away from the edge and away from places where slanted and vertical truss members joined the ceiling joists. A horizontal joist down the middle of the section allowed an estimation of how much of the ceiling framing effect in Table 2 is due to effects just over the ceiling joists. Configuration D has negligible joist effect so it was not modeled. The two-layer fiberglass batt configuration was modeled first. At Condition W2, the model predicts a framing effect of 0.01 vs. 0.19 to 0.21 for the whole ceiling in Table 4 for Configuration A, a difference of 0.18 to 0.20. This model does not account for the effects of the vertical and slanted truss members that penetrate the uniform covering of insulation. Visual inspection of the gaps caused by these members showed that the gaps extended between the full-width second layers of batts for over 60% of the length from eave to ridge. As Fig. 5 shows, not much disturbance is caused by the ceiling joists alone so the small framing effect from the model is reasonable because the insulation's thermal conductivity and the wood joist's thermal conductivity are not too different. The framing effect from Table 2 shows that the gaps caused by the vertical and slanted truss members have a significant effect for Configuration A. There are no such gaps in Configuration D to help explain its framing effect in Table 2. However, in addition to

the effect of the vertical and slanted truss members, 17% less insulation near the ridge could account for the rock wool's framing effect of 0.19 to 0.30.

Another run of the HEATING 7.2 model for the ceiling joist effect was done for PEPs on top of a layer of fiberglass. The gap between PEPs was as shown for Configuration B in Fig. 5. The predicted framing effect for the ceiling joists alone was 0.23 compared to 0.41 to 0.47 in Table 2 for the whole ceiling in Tests W1B, W2B and W3B (Configuration B without the extra sheathing), a difference of 0.18 to 0.24. A final run of this model had 4 in. (10.2 cm) square blocks of EPS on top of the space between the PEPs over the joists. A framing effect of 0.18 was predicted, compared to 0.32 to 0.34 in Table 2 for W2Bxb and W2Bxv, a difference of 0.14 to 0.16

A graphic comparison between the ceiling and the predicted framing effects is shown in Fig. 21. Again, the effect appears of the slightly high measured heat flow for Run W1A, which was noted in Fig. 19. A relatively high ceiling heat flow makes for a smaller $R_{ceiling}$ and a relatively high framing effect for this case, so the trend from W1A to W2A and W3A is not the same as from W1B to W2B and W3B. The difference between the ceiling and predicted framing effects is about the same for insulation Configurations A and B, which is consistent with a uniform effect of the vertical and slanting truss members. The difference is slightly smaller for Configuration Bx with sheathing over both the ceiling joists and the joints between PEPs. Here $FE_{ceiling}$ in Table 2 and Fig. 21 for Tests W2Bxb and W2Bxv displays the success of attempts to cover all the flaws preventing uniform coverage by PEPs. It is reasonable that the model comes closer to the measured results because the model has no effects of joints between PEPs while the experiments had the joints covered by EPS. Also, the same size of EPS blocks was used to span the space between PEPs over the joists in the model and the experiment.

5.3. WHOLE HOUSE MODEL

Although the use of the edge cap in Fig. 20 and vertical and truss sheathing in Fig. 17 show significant decreases in heat flows across the edge, overall savings are not significant enough to justify installation of them for the edge alone. To verify this insight, a model of an entire mobile home was specified for the public domain program, ASEAM 3.0, which uses the simplified energy analysis afforded by a modified bin method to predict annual energy use for residential and small commercial buildings (ACEC 1991). The base case for ASEAM 3.0 was a mobile home located in the southeastern U.S., heated and cooled by an electric air-to-air heat pump. The unit had nominal R_{US}-14 (R_{SI}-2.5) insulation in the roof/ceiling, R_{US}-11 (R_{SI}-1.9) in the side and end walls, and R_{US}-7 (R_{SI}-1.2) under the floor. The ceiling and floor joists were specified to be 24 in. (0.61 m) o.c. while the studs were 16 in. (0.41 m) o.c. Single pane windows occupied 10% of the wall area and a 15% framing factor was assumed for the walls to allow for the studs and framing for the windows and a single door. The results in Fig. 20, when incorporated into the whole wall and roof of a 14 ft wide × 52 ft long (4.3 m wide × 15.8 m long) mobile home, improve the R-value of the wall by 0.5% and that of the roof by 1.5%. ASEAM 3.0 shows that annual savings are only 15 to 22 KWh; not enough at the assumed $0.08/KWh for electricity to justify the investment needed for the foam cap. According to the results from further use of ASEAM 3.0, installation of 0.5 in. (13 mm)

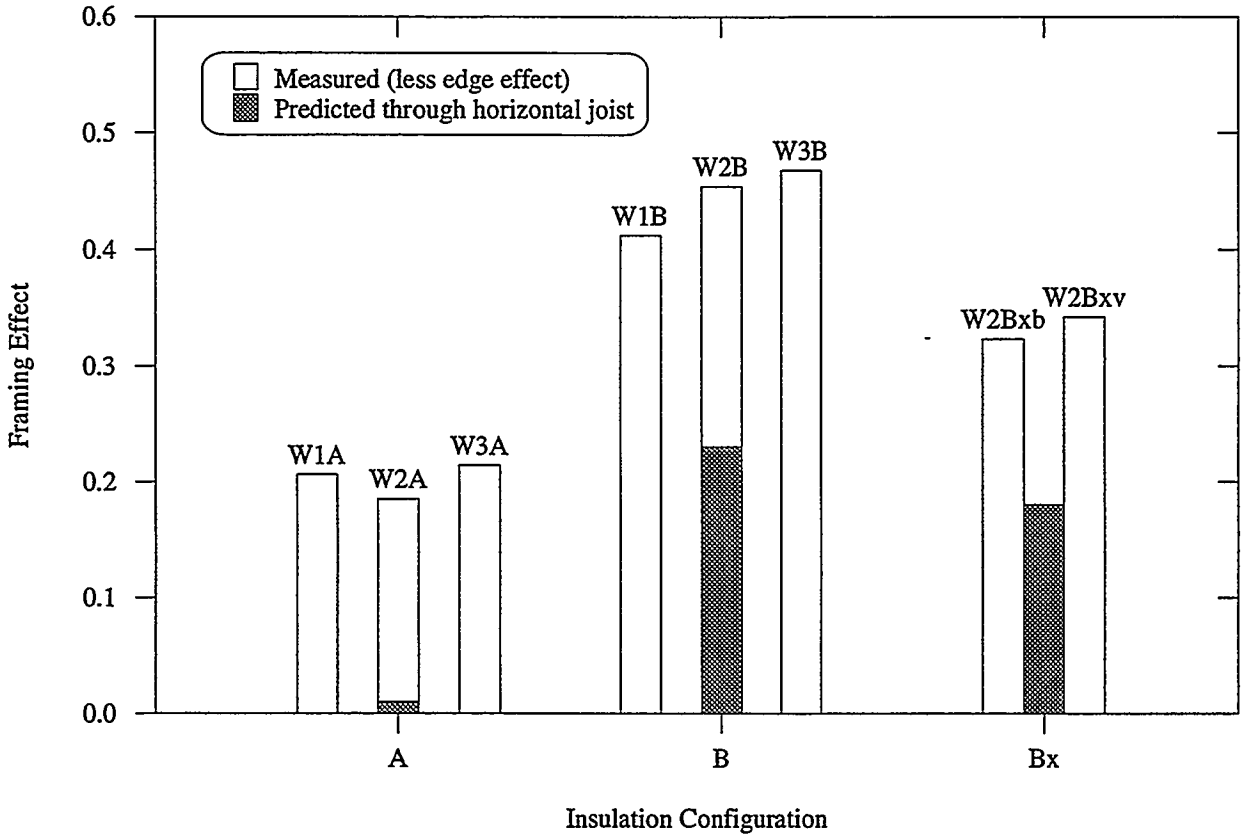

Fig. 21. Comparison between actual and predicted framing effects for insulation Configurations A, B and Bx.

thick (nominal R_{US}-2.5 or R_{SI}-0.44) sheathing on all outside walls and protection of the vertical part of the edge achieved simple payback times from 2.5 to 3 years when the long sides of the house faced east and west and 3 to 4 years when they faced north and south. Although 0.75 in. (19 mm) thick sheathing was used in the experiments, our industrial CRADA partner judged it too thick for adding on to a manufactured home with the existing roof to wall strapping requirements for mechanical strength. The edge protection in the vertical direction was assumed to be done at no additional cost by using scraps of fiberglass and sheathing at the eave edge instead of PEPs and the special foam cap. Sheathing for the walls was estimated to add a cost of \$0.135/ft² (\$1.25/m²).

6. SUMMARY AND CONCLUSIONS

Different insulation configurations with fiberglass batts and blown-in rock wool insulation in a test section like half the roof of one type of manufactured home showed the effects of reduced insulation R-value and a thermal bridge at the eave edge of the roof. The systems comprising a layer of fiberglass batts and PEPs (Configuration B) on the ceiling or blown-in rock wool (Configuration D) were not affected by vertical compression of insulation at the eave. Insulation coverage was poor over the joists with PEPs on top of fiberglass batts because the panels had to fit between the vertical and slanted truss members. There were also joints between the three panels used from eave to ridge in each space between joists. The thickness of the blown-in insulation at the edge was not as great as in the middle of the test section because of the short heel at the eave edge. Nor was it as thick at the ridge edge due to the blowing technique that was used. The configurations comprising two (Configuration A) and four (Configuration C) layers of fiberglass batts had compressed insulation at the eave but insulation was continuous from eave to ridge. Joist coverage was affected because the full-width batts had to bend around the vertical and slanted truss members.

Thermal performance of the Configurations A, B, C and D is as follows. The ratios of the system to center-of-cavity insulation R-values show how much the system R-values are affected by insulation compression or reduced insulation at the eave edge, thermal bridges and effects through joists and joints.

Configuration	Condition	Center-of-Cavity R_{US} (R_{SI})	System R_{US} (R_{SI})	System/Center (%)
A. Two FG Batts	Winter	15.6-17.2 (2.7-3.0)	12.0-12.4 (2.1-2.2)	72-77
	Summer	13.2 (2.3)	12.1 (2.1)	92
B. PEPs on FG	Winter	24.1-25.8 (4.2-4.5)	12.4-12.7 (about 2.2)	49-53
	Summer	---	---	---
C. Four FG Batts	Winter	30.4-31.7 (5.4-5.6)	16.8-18.6 (3.0-3.3)	55-59
	Summer	27.6 (4.9)	15.8 (2.8)	57
D. Rock Wool	Winter	13.0-14.0 (2.3-2.5)	9.1-10.1 (1.6-1.8)	65-74
	Summer	12.4 (2.2)	9.9 (1.8)	80

Improvements in system R-values were sought by improvements in Configurations B, C and D. After the initial tests with Configuration B, 0.75 in. (1.9 cm) thick extruded polystyrene (XPS) sheathing was installed over the eave edge and 4 in. (10.2 cm) thick EPS was installed over most of the underprotected joists and over the joints between the PEPs. The sheathing improved the system R-value by 23% compared to the initial results with Configuration B. Vertical XPS sheathing at the eave edge improved the system R-value for Configuration C by 9%. Placing two EPS layers, each 0.625 in (1.6 cm) thick, over the trusses instead of the metal roof showed a 7 to 9% increase over the base-case system R-values with

Configuration D. Adding an aluminum foil facing the attic space showed a 27% increase at winter conditions and a 29% increase at summer conditions relative to the base results. Placing PEPs instead of one of the EPS layers over the trusses yielded 28% improvement over Configuration D at winter conditions and 51% at summer conditions. In all these cases, the eave edge was left thermally underprotected. The entire eave edge was then protected by wide EPS boards like the one covering most of the stub wall. The combined effect of all improvements was a 51% higher system R-value at the mid-winter condition and a 95% higher one at the summer condition relative to the base-case system R-values with Configuration D.

HUD manufactured housing construction and safety standards impose an upper limit on the overall U value of the roof/ceiling, walls and floor. The limit varies with location. For the roof/ceiling, center-of-cavity insulation R-values and inside and outside film resistances, all at 75°F (24°C), are used with parallel path corrections for insulation compression and framing effects. For this test section, including the stub wall on the eave edge, the system R-value for insulation Configuration A by the HUD method is estimated to be R_{US}-14.8 (R_{SI}-2.6). This is 21% higher than the measured average of 12.2 for this system.

The eave edge, the space around a horizontal ceiling joist, and an entire 14 ft (4.3 m) wide × 52 ft (15.8 m) long manufactured home were modeled to provide insight to the measurements. For the two layer fiberglass batt insulation package and for the PEPs over fiberglass batts, the model of the eave edge showed that 16% of the total heat flow through the test section came through the eave edge. For the rock wool insulation, the eave edge loss was 13% of its greater total heat loss. For the two-layer fiberglass batt and PEP configurations, a model of heat flow through a horizontal ceiling joist addressed only the joist effect in the ceiling R-values. The joist was away from the eave edge and free from interference by vertical and slanted trusses. Ceiling R-values were obtained from differences between measured total heat flows and predicted eave edge heat flows. For the PEPs, further modeling addressed the effects of sheathing over the joist. The blown-in rock wool was not modeled because it would not show a joist effect. The predictions yielded a joist effect of only 1% for the two layers of fiberglass batts but, since the PEPs did not cover the joists, about 18% and 23% for the PEPs with and without sheathing, respectively. The differences between the joist and total ceiling framing effects were about 20% for all of the fiberglass configurations meaning that the vertical and slanted truss members effectively reduced the system value by about 20% from the center-of-cavity insulation value. The blown-in rock wool showed a 19 to 30% framing effect for the ceiling, which is attributed to poorer coverage near the ridge edge and some effect of the vertical and slanted trusses.

The whole house computer simulation showed annual energy savings for proposed improvements in construction features of manufactured homes. Improving just the edge of the roof saved very little. But, if mechanical constraints would allow the extra width caused by 0.5 in. (13 mm) thick vertical XPS sheathing over all exterior walls and the top of the trusses at the eave edge, the cost of the sheathing could be recovered in payback times of 2.5 to 4 years.

The PEPs available for the tests achieved R_{US}-16 h·ft²·°F/BTU (R_{SI}-2.8 m²·K/W) in 0.79 in. (20 mm) thickness. This is very good center-of-cavity performance. The measurements of system R-value with PEPs between the trusses on top of a layer of fiberglass batts showed too many thermal shorts to take economic advantage of the high center-of-cavity R-value. The measurements of system R-value with insulation over the trusses showed potential for improving thermal performance of the roof cavity if the eave edge is improved simultaneously. PEPs could have application near the eave edge where space is very cramped if they can be installed without danger of damage to them. This danger is not easy to avert because there are strict requirements for strapping the roof to the side walls. For the near term, conventional sheathing, as much as can be tolerated, is recommended over the walls and the eave edge of the trusses.

REFERENCES

ACEC. 1991. ASEAM-3.0, a Simplified Energy Analysis Method: Program and User's Manual. Washington, DC: American Consulting Engineers Council Research and Management Foundation.

ASHRAE. 1993. *1993 ASHRAE Handbook--Fundamentals*, Chaps. 20 (Fig. 2), 22, 36. Atlanta: American Society of Heating, Refrigerating and Air-Conditioning Engineers, Inc.

ASTM. 1989. ASTM C 236-89, Standard test method for steady-state performance of building assemblies by means of a guarded hot box, pp. 53-63, Vol. 04.06, *Annual Book of ASTM Standards*. Philadelphia: American Society for Testing and Materials.

ASTM. 1991. ASTM C 518-91, Standard test method for steady-state heat flux measurements and thermal transmission properties by means of the heat flow meter apparatus, pp. 153-164, Vol. 04.06, *Annual Book of ASTM Standards*. Philadelphia: American Society for Testing and Materials.

ASTM. 1992a. ASTM C 653-92, Standard guide for determination of the thermal resistance of low-density mineral fiber insulation, pp. 251-255, Vol. 04.06, *Annual Book of ASTM Standards*. Philadelphia: American Society for Testing and Materials.

ASTM. 1992b. ASTM C 578-92, Standard specification for rigid, cellular polystyrene thermal insulation, pp. 203-207, Vol. 04.06, *Annual Book of ASTM Standards*. Philadelphia: American Society for Testing and Materials.

Childs, K. W. 1993. Heating 7.2 Users' Manual. Oak Ridge National Laboratory Report No. ORNL/TM-12262. Oak Ridge, TN: Oak Ridge National Laboratory.

Coleman, H. W., and W. G. Steele. 1989. *Experimentation and Uncertainty Analysis for Engineers*, Chaps. 1-2. New York: J. Wiley and Sons.

Conner, C. C., and Z. T. Taylor. 1992. Overall U-values and heating/cooling loads - manufactured homes. U.S. Department of Housing and Urban Development Report No. DOC-0005945. Rockville, MD: U.S. Department of Housing and Urban Development.

Desjarlais, A. O., D. W. Yarbrough, D. L. McElroy, and R. P. Tye. 1980. An experimental study of thermal resistance values (R-values) of low density mineral fiber building insulation batts commercially available in 1977, Oak Ridge National Laboratory Report ORNL/TM-7266. Oak Ridge, TN: Oak Ridge National Laboratory.

McElroy, D. L., D. W. Yarbrough, and R. S. Graves. 1987. The thickness and density of loose-fill insulations after installation in residential attics, pp. 493-505, *Thermal Insulation: Materials and Systems*. ASTM STP 922, F. J. Powell, and S. L. Matthews, Eds. Philadelphia: American Society for Testing and Materials.

Sparrow, E. M., and R. D. Cess. *Radiation Heat Transfer, Revised Edition,* Table 2.2. Belmont, CA: Brooks/Cole Publishing Co.

Wilkes, K. E. 1979. Thermophysical properties data base activities at Owens-Corning Fiberglass. *Proceedings of the 1979 ASHRAE/DOE-ORNL Conference on the Thermal Performance of the Exterior Envelope of Buildings,* pp. 662-677. Atlanta: American Society of Heating, Refrigerating and Air-Conditioning Engineers, Inc.

Wilkes, K. E. 1995. Private Communication. Oak Ridge, TN: Oak Ridge National Laboratory.

Yarbrough, D. W., and I. A. Toor. 1983. Effect of air movement on thermal resistance of loose fill thermal insulations, pp. 529-541, *Thermal Insulation: Materials and Systems for Energy Conservation.* ASTM STP 789, F. A. Govan, D. M. Greason, and J. D. McAllister, Eds. Philadelphia: American Society for Testing and Materials.

INTERNAL DISTRIBUTION

1. G. L. Akers
2. E. L. Blaylock
3-7. P. W. Childs
8. K. W. Childs
9-10. J. E. Christian
11. G. E. Courville
12. A. O. Desjarlais
13. S. K. Fisher
14. S. B. Floyd
15. M. B. Gettings
16. S. B. Heth
17-22. J. Kośny
23. W. P. Levins
24. P. J. Lewis
25. P. M. Love
26. H. A. McLain
27. V. C. Mei
28. C. L. Moody
29. C. I. Moser
30-35. R. R. Parks
36-56. T. W. Petrie
57. R. B. Shelton
58. R. L. Shelton
59. J. H. Sorenson
60. R K. Tallent
61. T. J. Wilbanks
62-63. K. E. Wilkes
64. S. B. Wright
65. J. Vancoevering
66. ORNL Patent Office
67. Central Research Library
68. Document Reference Section
69-70. Laboratory Records
71. Laboratory Records - RC

EXTERNAL DISTRIBUTION

72. James L. Anderson, Foam Enterprises, Inc., 13630 Watertower Circle, Minneapolis, MN 55441
73. Gregory J. Andrews, Tennessee Technological University, Dept. of Chemical Engineering, Box 5013, Cookeville, TN 38505
74. Erv Bales, University Heights, New Jersey Institute of Technology, Newark, NJ 07102
75. Mark Bomberg, National Research Council Canada, 2008 Quincy Avenue, Gloucester Canada K1A 6B5
76. Jean Boulin, U. S. Dept. of Energy, EE-432, 5E-080/FORSTL, 1000 Independence Avenue, S.W., Washington, D.C. 20585-0121
77. Jeff Brisley, Knauf Fiber Glass, 240 Elizabeth Street, Shelbyville, IN 46176
78. Barton W. Bromley, American Rockwool, Inc., P. O. Box 880, Spring Hope, NC 27882
79. Carl Dakin, Dakin Law Tech, 384 Inverness Drive, Suite 205, Inglewood, CO 80112

80. Clayton DeKorne, Journal of Light Construction, RR2, Box 146, Richmond, VT 05477
81. Thomas E. Drabek, Professor, Department of Sociology, University of Denver,1Denver, Colorado 80208-0209
82. Rene M. Dupuis, Structural Research, Inc., 3213 Laura Lane, Middleton, WI 53562
83. Floyd England, England & Associates, P.O. Box 154578, Waco, TX 76715
84. William Freeborne, Dept. of Housing & Urban Development, 451 7th Street SW, Rm. 8138, Washington, D.C. 20410
85. Smith A. Funk, Celotex Roofing Products, 4010 Boy Scout Blvd., Tampa, FL 33607-5750
86. Leon R. Glicksman, Massachusetts Institute of Technology (M.I.T.), 4-209, 77 Massachusetts Avenue, Cambridge, MA 02139
87. William Goss, Mechanical Engineering Dept., University of Massachusetts, Amherst, MA 01003
88-89. Ronald S. Graves, R&D Services, Inc., 1770 Spring Road, Lenoir City, TN 37771
90. Joseph Hagan, Center for Applied Engineering, 10301 Ninth Street North, St. Petersburg, FL 33716
91. Robert Hageman, Kool Ply Company, 311-D E. St. Elmo, Austin, TX 78745-1249
92 David Harris, National Institute of Building Sciences, 1201 L Street, N.W., Suite 400, Washington, D.C. 20005
93. Donna M. Hawkins, Dept. of Energy, EE-40, 6A-081/FORSTL, 1000 Independence Avenue, S.W., Washington, D.C. 20585-0121
94. Stephen G. Hildebrand, Director, Environmental Sciences Division, Oak Ridge National Laboratory, P. O Box 2008, Oak Ridge, TN 37831-6037
95. Bion Howard, 14513 Kent Drive, Upper Marlboro, MS 20772-7772
96. Richard H. Karney, Director, Building Systems and Materials Division, U. S. Department of Energy, EE-421, Rm. 5E-098/FORSTL, 1000 Independence Avenue SW, Washington, D.C. 20585-0121
97-100. E. Tyler Kelley, Clayton Homes, Inc., 164 Racoon Valley Road, Maynardville, TN 37807
101. William A. Kirn, Rohm and Haas Co., 727 Norristown Road, Spring House, PA 19477
102. Esher Kweller, U.S. Department of Energy, EE-422, Rm. 5H-048/FORS, 1000 Independence Avenue SW, Washington, D.C. 20585-0121
103. Harold G. Lorsch, Center for Insulation Technology, Drexel University, Philadelphia, PA 19104
104. Peter Lund, NEMO 2, Helsinki University of Technology, Otakaari 3, FIN-02150 Espoo, Finland
105. Robert F. Martin, Roof Maintenance Systems, P.O. Box 67, Farmingoak, NJ 07727
106. William F. Martin, Roof Design Works, Inc., 5516 Renford Drive, Knoxville, TN 37919
107. Merle F. McBride, Owens-Corning Fiberglas, 2790 Columbus Road, Granville, OH 43023-1200

108. R. Gerry Miller, Center for Applied Engineering, Inc., 10301 9th Street, N., St. Petersburg, FL 33716
109. Dave Mowry, Applegate Insulation, 1000 Highview Drive, Webberville, MI 48892
110. NCAT Library, National Center for Appropriate Technology, P.O. Box 3838, Butte, MT 59702
111. Ned Nisson, Energy Design Update, 235 W. 102nd Street, #7J, New York, NY 10025
112. David G. Ober, Miami Testing Laboratory, 1640 West 32nd Place, Hialeah, FL 33012
113. Frank J. Powell, 12218 Cattail Lane, Jacksonville, FL 32223
114. Richard Ray, Schuller International, Inc., P.O. Box 625005, Littleton, CO 80162-5005
115. Carsten Rode, Danish Building Research Institute, P.O. Box 119, Dr. Neergaards Vej 15, Horsholm, Denmark DK-2970
116. W. J. Rossiter, National Institute of Science & Technology (NIST), Bldg. 226, Rm. B348, Gaithersburg, MD 20899
117. Cliff Shirtliffe, C.J. Shirtliffe & Associates, 9 Blue Spruce Court, Gloucester, Ontario, Canada K1B 3E3
118. Paul H. Shipp, USG Corporation, 700 N. Highway 45, Libertyville, IL 60048
119. Tom Smith, National Roofing Contractors Assoc., O'Hare International Center, 10255 W. Higgins Road, Suite 600, Rosemont, IL 60018-5607
120. George F. Sowers, Senior Vice President, Law Companies Group, Inc., 114 Townpark, Drive, Suite 250, Kennesaw, GA 30144-5599
121. William R. Strzepek, Dow U.S.A., P. O. Box 515, Granville, OH 43023
122. Bob Swisher, Dow Corning, 1225 Northmeadow Pkwy, #104, Roswell, GA 30076
123. Jim Syferd, American Rockwool, Inc., P. O. Box 880, Spring Hope, NC 27882
124. Anton Ten Wolde, Forest Products Laboratory, One Gifford Pinchot Drive, Madison, WI 53705-2398
125. John Talbott, U.S. Dept. of Energy, EE-421, Rm. 5E-098/FORSTL, 1000 Independence Avenue, S.W., Washington, D.C. 20585-0121
126. Timothy Tong, Dept. of Mechanical & Aerospace Eng., Arizona State University, Tempe, AZ 85287
127. George Tsongas, Portland State University, Mechanical Engineering Dept., Portland, OR 97207-0751
128. Adrian Tuluca, Steven Winter Associates, Inc., 50 Washington Street, Norwalk, CT 06854
129. R. P. Tye, 292 Jerusalem Road, Choasset, MA 02025
130. Martha G. Van Geem, Construction Technology Laboratory, 5420 Old Orchard Road, Skokie, IL 60077
131. C. Michael Walton, Department of Civil Engineering, University of Texas at Austin, Austin, TX 78712-1076
132. James R. Wells, Owens-Corning Fiberglas, 2790 Columbus Road, Granville, OH 43023
133 David Williams, Dow Chemical, P.O. Box 515, Granville, OH 43023
134-135. David W. Yarbrough, Tennessee Technological University, Dept. of Chemical Engineering, Box 5013, Cookeville, TN 38505

136. Robert R. Zarr, National Institute of Standards and Technology, Bldg. 226, B320, Gaithersburg, MS 10899
137. ORNL, Site Manager, U.S. Department of Energy, Oak Ridge National Laboratory, P.O. Box 2008, Oak Ridge, TN 37831-6269
138-188. BTESM Library, Oak Ridge National Laboratory, PO Box 2008, Bldg. 3114, Oak Ridge, TN 37831-6070
189-190. OSTI, U.S. Dept. of Energy, PO Box 62, Oak Ridge, TN 37831